Static and Kinematic Absolute GPS Positioning and Satellite Clock Error Estimation

by

Shin-Chan Han

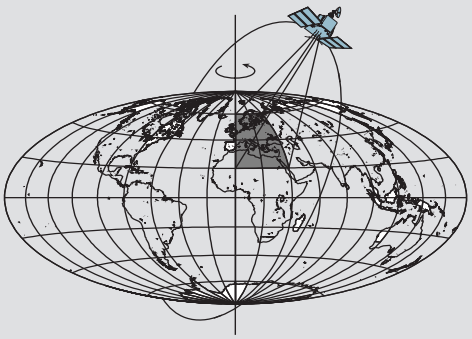

Report No. 454

Geodetic Science and Surveying
Department of Civil and Environmental Engineering and Geodetic Science
The Ohio State University
Columbus, Ohio 43210-1275

April 2000

Precision Absolute GPS Positioning through Satellite Clock Error Estimation

By

Shin-Chan Han

Report No. 454

Geodetic Science and Surveying
Department of Civil and Environmental Engineering and Geodetic Science
The Ohio State University
Columbus, Ohio 43210-1275

April 2000

ABSTRACT

This study presents the results of investigations to determine accurate position coordinates using the Global Positioning System in the absolute (point) positioning mode. The most common method to obtain accurate positions with GPS is to apply double-differencing procedures whereby GPS satellite signals are differenced at a station and these differences are again differenced with analogous differences at other stations. The differencing between satellites eliminates the receiver clock errors, while the between-station differences eliminate the satellite clock errors (as well as other errors, such as orbit error). However, only coordinate differences can be determined in this way and the accuracy depends on the baseline length between cooperating stations. The strategy with accurate point positioning is to estimate GPS satellite clock errors independently, thus obviating the between-station differencing. The clock error estimates are then used in an application of a single-difference (between-satellite) positioning algorithm at any site to determine the coordinates without reference to any other site. Using IGS (International GPS Service) orbits and station coordinates, the GPS clock errors were estimated at 30-second intervals and these estimates were compared to values determined by JPL (Zumberge et al., 1998). The agreement was at the level of about 0.1 nsec (3 cm).

The absolute positioning technique was tested in an application of a single-differenced (between-satellite) positioning algorithm in static and kinematic modes. For the static case, an IGS station was selected and the coordinates were estimated. The estimated absolute position coordinates and the published values had a mean difference of up to 18 cm with standard deviation less than 2 cm. For the kinematic case, data (every second) obtained from a GPS buoy were tested and the result from the absolute positioning was compared to a DGPS solution. The mean difference between the two algorithms is less than 40 cm and the standard deviation is less than 23 cm. It was proved that a higher rate (less than 30 sec.) of satellite clock determination and a good tropospheric delay model are required to do absolute kinematic positioning to better than 10 cm accuracy.

PREFACE

This report was prepared by Shin-Chan Han, a graduate student, Department Civil and Environmental Engineering and Geodetic Science, under the supervision of Professor Christopher Jekeli. This research was supported by the National Imagery and Mapping Agency under Air Force Phillips Laboratory contracts F19628-95-K-0020 and F19628-96-C-0169.

This report was also submitted to the Graduate School of Ohio State University as a thesis in partial fulfillment of the requirements for the Master of Science degree.

ACKNOWLEDGMENTS

Most of all, I wish to express my deep gratitude to my adviser, Dr. Christopher Jekeli for his support, encouragement, patience and intellectual insight throughout this research. I would like to express my sincere thanks to Dr. C. K. Shum for thoughtful comments, suggestions, and providing access to the Lake Michigan GPS-Buoy campaign data.

TABLE OF CONTENTS

PAGE

LIST OF TABLES

LIST OF FIGURES

1 Introduction

The Navigation Satellite Timing and Ranging Global Positioning System (NAVSTAR GPS) has been developed and is being operated to support accurate position, velocity, and time by the Department of Defense (DoD). It is a global, all-weather, and space-based 24-hour operational navigation system (Wooden, 1985).

The 18 GPS satellites were anticipated to be placed in an orbital configuration to optimize a spatial and temporal global coverage between 1986 and 1990 (Jorgensen, 1984). The plan called for placing three satellites (120° apart) in each of six evenly spaced orbital planes. These orbits are nearly circular, inclined at 55°, and had 12-hour sidereal periods (Remondi, 1985). Presently, the constellation consists of 24 operational satellites (at 20,200 km altitude) deployed in six evenly spaced planes (A to F) with 55° inclination and four satellites per orbital plane. In addition, four active spare satellites for replenishment are operational (Graviss, 1992).

Each GPS satellite transmits its position and other navigational information via the L-band radio signals, L1 (1575.43 mHz) and L2 (1227.60 mHz). The L-band carrier signal is modulated with data carrying information such as the satellite status, the satellite clock error and the ephemeris (Hofmann-Wellenhof et al., 1997). The L1 carrier signal is modulated with a precision code (P-code), known as the precise positioning service (PPS) code, and a coarse acquisition code (C/A-code), known as the standard positioning service (SPS) code. On the other hand, the L2 carrier signal is modulated with only the PPS code (Remondi, 1985).

The PPS and SPS code has a chipping rate of 10.23 mHz and 1.023 mHz, respectively, and with respective repeat periods of 37 weeks and 1 millisecond (Spilker, 1978). The C/A-code for SPS has a wavelength of 300 meters, while the P-code for PPS has 30 meter wavelength. The noise level for the P-code is less than 0.3 meters and less than 3 meters for the C/A-code.

There are two intentional degradations which contribute to the GPS positioning inaccuracy. The first one is called Anti-Spoofing (AS). AS allows GPS to conceal the precision code and to issue an encrypted code, which prevents non-authorized users from using the full capability of the PPS. AS is performed by the modulo-2 addition of the precision code and an encryption W-code (Leick, 1995). The resulting Y-code is the signal transmitted and modulated on the L1 and L2 carriers.

The other method used to degrade the GPS positioning accuracy is the Selective Availability (SA). SA intentionally corrupts the navigation information by dithering the fundamental frequency of the satellite clock (δ-process) and by manipulating the ephemeris data (ε-process). The accuracy is decreased to 100 meters for a horizontal position and 140 meters for a vertical position. The accuracy of satellite clock error is decreased to a level of 340 ns within 95% probability level (Parkinson et al., 1996).

Using the broadcast orbits and clocks which are already affected by SA, Heroux and Kouba (1995) tested single point positioning with one receiver and obtained expected

poor results. During the 25 minute time segment, the RMS of the variations with respect to the averaged latitude, longitude and height were 22, 15 and 65 meters.

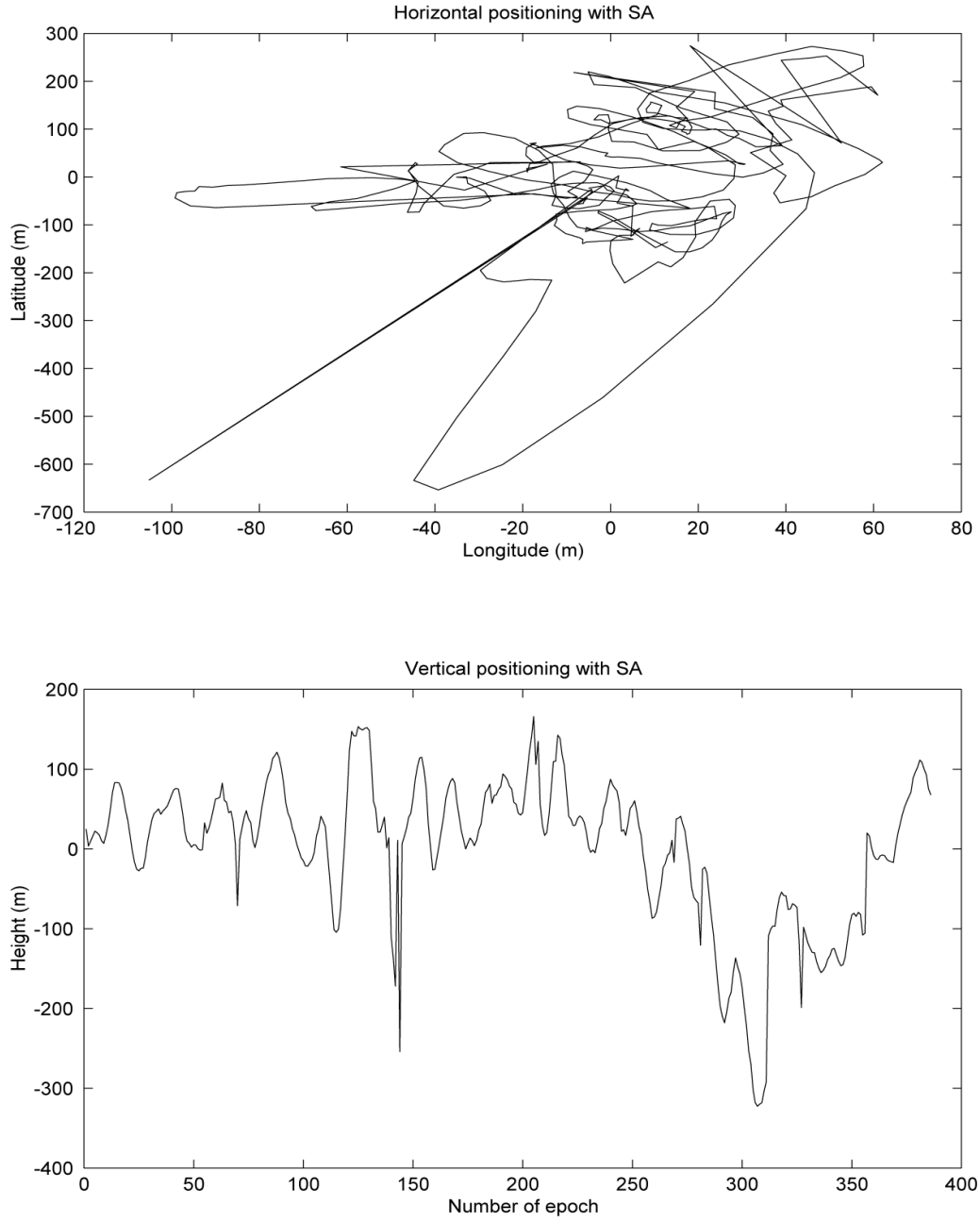

Figure 1.1: Static positioning variation due to SA; horizontal (top) & vertical (bottom)

Figure 1.1 shows an example of the absolute positioning solved every 30 seconds during approximately 3 hours using the broadcast navigation message with both C/A- and P2-code. The positioning is affected mainly by SA, which causes the position to vary systematically with respect to time. The standard deviation of the horizontal and vertical positioning is about 70 meters and 90 meters.

The δ–process in SA has the same impact on the code and the phase since the fundamental frequency is dithered. According to Parkinson et al. (1996), the clock accuracy with and without Selective Availability is 40 ns (12 m) and 340 ns (100 m), respectively. The positioning accuracy, therefore, can be improved nine times if the satellite clock error is known.

Figure 1.2 indicates the satellite (PRN1) clock error estimates at 12/5/1998 (Chapter 3). The clock was affected by the Selective Availability, specifically the δ-process. The precise satellite clock error estimates in the figure include not only the drift, but also the high fluctuation which degrades the broadcast clock information up to 60 m. The value of the estimated satellite clock error at the 16th epoch in Figure 1.2 is seen to be 66.65 microseconds, while the navigation message clock information gives 66.45 microseconds. The difference between them causes around 60 m range error.

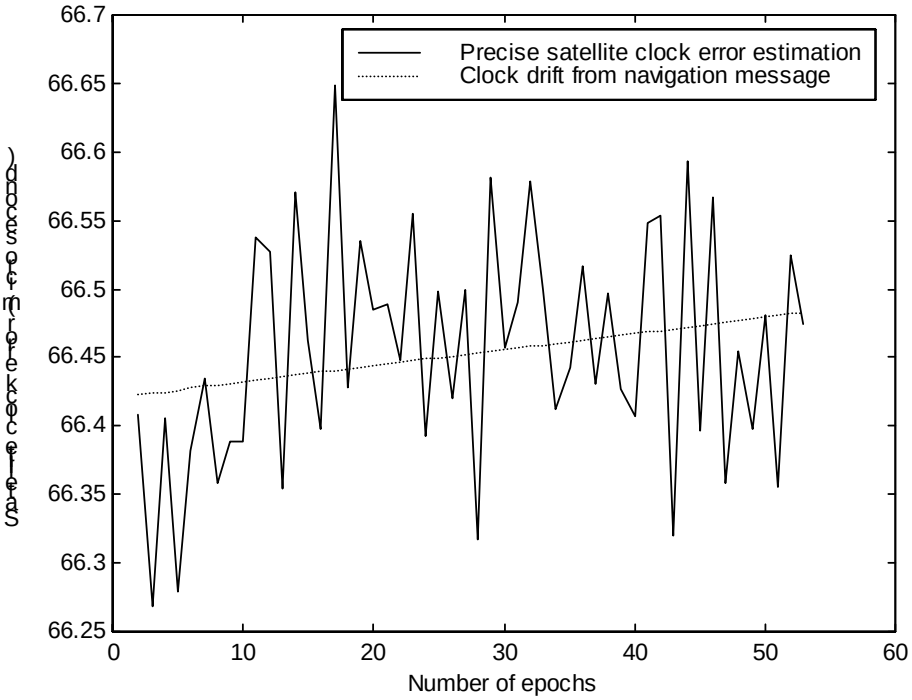

Figure 1.2: The precisely estimated satellite clock error (one epoch for 30 sec)

As seen above, one of the important unknowns in GPS positioning is the satellite clock error, which is defined as the variation of the nominal time (the reading of the

satellite clock) with respect to GPS time. GPS time is defined by the cesium clocks of the control segment station and agreed with UTC in January 1980 (Torge, 1991). Part of the satellite clock error is due to random errors in the clocks and partly it is an intentional dithering (SA), that degrades the signal accuracy up to 100 meters. Geodesists have circumvented this error by using differential techniques whereby the signals from satellites at two stations are differenced (Section 2.2.3), thus eliminating the common satellite and receiver clock errors (defined as difference between the receiver clock reading and GPS time). In addition, GPS orbit errors also tend to cancel in the case of receiver single-difference and double-difference (about 10 cm error for baseline length of 100 km; Leick, 1995). However, the relative positioning of one station with respect to the other has its limitations and the accuracy depends strongly on the baseline length between stations (10 km for decimeter accuracy, Hofmann-Wellenhof et al., 1997).

The primary reason to limit the baseline length is to reduce the differential effect of the atmospheric refraction, i.e., the ionospheric and tropospheric delays of the signal. One of the critical aspects in GPS positioning is the accurate modeling of the tropospheric effect at the two stations, where errors in the model do not cancel if the stations are far apart (several hundreds km). In order to reduce the differential ionospheric effect over a long baseline, Goad and Yang (1997) calculated the autocorrelation function for the double-differenced ionospheric delay. They then estimated the static position of one station epoch-by-epoch as if it were kinematic with the baseline length of about 179 km. Their results showed a few cm precision at each coordinate.

Instead of double-differencing between two receivers, precise absolute positioning with only one receiver can be achieved in either the static or the dynamic mode, if the satellite clock errors and the orbits are determined with sufficient accuracy. This has tremendous importance in many applications in geodesy and other disciplines that require accurate positioning in remote areas. The quality of the orbits and clock errors calculated from the navigation message, however, are not accurate enough for accurate absolute positioning because of the impact of SA. Therefore, it is necessary to estimate precise GPS orbits and clock errors in order to conduct accurate absolute positioning.

Nowadays, the International GPS Service (IGS) provides GPS satellite orbits and clock error estimates at 900-second intervals with about 5 and 10 cm accuracy, respectively and they are available after two weeks (IGS, 1999). However, it should be noted that orbital state vectors and clock errors at a much higher rate (up to 1 Hz) are required in some applications requiring accurate positioning of moving-base platforms such as aerial photogrammetry, sea-level monitoring using ocean buoys, airborne vector gravimetry, and other remote sensing systems.

GPS ephemerides at higher rates, such as 30 sec (0.033 Hz), equal to the observational data rate of the current IGS stations, can be obtained by an interpolation of the 900-sec ephemerides within centimeter level accuracy (Remondi, 1989, 1991). However, the interpolation is not feasible to obtain the satellite clock errors because the SA effects on the clock errors have significant variations as seen in Figure 1.2. In this study, a new method is introduced (for application to post-processing and interpolated orbits) to estimate the satellite clock error every 30 sec using the observations from the globally distributed IGS control stations (IGS, 1999).

Once the satellite clock error is determined, precise absolute positioning can be performed by using these estimates. The absolute positioning technique has no limitation in baseline length caused by the first degree ionospheric effect because the algorithm uses the ion-free phase combination (Section 3.2 in Chapter 3). However, higher-order ionospheric effects and un-modeled tropospheric effects still remain. In absolute positioning, GPS clock errors are estimated from globally distributed IGS stations around the surveying area, and then the positions with the estimated GPS clock errors are estimated epoch-by-epoch. This procedure will be developed in Chapter 3.

Similar research in absolute positioning has already been performed. Mur (1995) separated the clock error into a clock bias for the first epoch and a clock drift, and estimated them by using pseudo-range and phase observables, respectively. In order to check the quality of the clock error estimates, he performed pseudorange point positioning of selected IGS stations with these estimates every 30 seconds. The typical horizontal RMS difference with the known coordinates was on the order of 0.6 m and the vertical RMS difference with the known coordinates on the order of 1.2 m. Some biases (around 1 m) in each coordinate were found as well.

Lachapelle et al. (1996) performed aircraft absolute point positioning using GPS post-mission orbits and satellite clock error estimates, and compared the absolute positioning results with DGPS solutions. The overall analysis showed that the post-mission absolute point positioning of the aircraft is possible within 1-2 meters RMS accuracy in latitude and longitude, and 3 meters RMS accuracy in height with single frequency GPS observables.

Zumberge et al. (1998) estimated the satellite clock error every 30 seconds with sub-decimeter accuracy, which is a factor of 100 to 1000 times better than the clock error estimates in the broadcast navigation message. Kinematic positioning of moving receivers with a 30-second data rate was achieved with a precision of approximately 7 cm 3D-RMS. However, the position errors at every 5 seconds were degraded to about 30 cm in the vertical coordinates.

This research focuses on the satellite clock error estimation and the subsequent use of these estimates to develop kinematic and static absolute GPS positioning algorithms. An independent, end-to-end algorithm is developed and results from its implementation are compared to clock estimates published by JPL. Static and kinematic GPS data at both 30 sec and 1 sec sampling rate from actual surveys are processed and compared with the known values and corresponding DGPS solutions.

2 Global Positioning System : overview and data modeling

2.1 GPS Observation Equations

GPS provides range and carrier phase measurements between the satellite and the receiver. However, these measurements are corrupted by errors caused by the atmosphere and the two non-synchronized clocks of the satellite and the receiver. Unlike electronic distance measurement (EDM) device, the signal transmitter and the receiver are different. GPS satellites transmit the signal and a receiver collects the signal. Therefore, the GPS signal can be distorted easily by both receiver and satellite clock errors. One calls this distorted range "pseudorange", which includes other systematic errors also. The pseudorange measurement is derived by the signal travel time between the satellite and the receiver and the carrier phase measurement is calculated by the phase difference between the incoming signal from the satellite and the signal generated by the receiver oscillator.

Ignoring other range errors, but not the satellite and receiver clock errors, the equations describing the pseudorange and the carrier phase follows (Hofmann-Wellenhof et al., 1997):

$$P_R^S = c[(t_R(GPS) + \delta_R) - (t^S(GPS) + \delta^S)] = \rho_R^S + c\Delta\delta_R^S, \tag{2.1}$$

where

P_R^S is the pseudorange measurement between the satellite, S and the receiver, R.

c is the speed of the light in vacuum.

$t_R(GPS) + \delta_R$ is the receiver clock reading at the signal reception moment.

$t^S(GPS) + \delta^S$ is the satellite clock reading at the signal transmission moment.

$t_R(GPS)$ is the GPS time at the signal reception moment.

$t^S(GPS)$ is the GPS time at the signal transmission moment.

δ_R is the deviation of the receiver clock reading from the GPS time and it is defined as the GPS receiver clock error.

δ^S is the deviation of the satellite clock reading from the GPS time and it is defined as the GPS satellite clock error.

ρ_R^S is the true range between the satellite and the receiver and can be accurately approximated by $c\left(t_R(GPS) - t^S(GPS)\right)$ because the GPS time is based on an accurate atomic time scale.

$c\Delta\delta_R^S$ is the range error caused by two clock errors.

For the carrier phase observation, one imports a beat phase, which is defined by the

difference between the satellite-generated phase and the receiver-generated phase.

$\varphi^S(t-\tau) = ft - f\frac{\rho}{c} - f\delta^S$; satellite-generated phase at signal transmission time

$\varphi_R(t) = ft - f\delta_R$; receiver-generated phase at signal reception time

where

f is the frequency of the L1 or L2 carrier phase.

τ is the signal travel time between the satellite and the receiver, which is equal to the true range divided by the speed of light, $\frac{\rho}{c}$.

t is the GPS time at the signal reception moment.

Therefore, the beat phase is given by

$$\varphi_R^S(t) = \varphi^S(t-\tau) - \varphi_R(t) = -f\frac{\rho}{c} - f\Delta\delta_R^S \tag{2.2}$$

where $\Delta\delta_R^S$ includes only the difference term between the two clock errors, assuming no other range errors or phase biases. If one assumes the satellite is tracked from t_0 to t, the beat phase can be represented as,

$$\varphi_R^S(t) = \Delta\varphi_R^S\Big|_{t0}^{t} + N_R^S \tag{2.3}$$

where $\Delta\varphi_R^S\Big|_{t0}^{t}$ is the value that the receiver measures at every epoch t, and N_R^S is an initial integer number, which is not known directly from the receiver data. Also this integer value remains constant if tracking is maintained without loss of lock. Now, let $\varphi_R^S = -\Delta\varphi_R^S\Big|_{t0}^{t}$, then the final form of carrier phase equation is

$$\varphi_R^S = \frac{1}{\lambda}\rho_R^S + \frac{c}{\lambda}\Delta\delta_R^S + N_R^S \tag{2.4}$$

where λ is the wavelength of the GPS carrier phase.

The phase can be measured to better than 0.01 cycles (Hofmann-Wellenhof, 1997). Two different frequencies are used in positioning to eliminate the ionospheric effect (section 2.3). The L1 carrier frequency is 1575.42 MHz corresponding to a wavelength of about 19.0 cm. The frequency and wavelength of the carrier L2 are 1227.60 MHz and 24.4 cm respectively. The characteristic of positioning with this relatively high frequency or short wavelength carrier is high resolution; however, there is the problem of solving an additional unknown, the ambiguity.

2.2 Mathematical Models for Positioning

2.2.1 Single Point Positioning

In the process known as single point positioning one determines the observer's position by using undifferenced GPS measurements. Suppose GPS pseudorange measurements P_i^j are corrupted only by two clock errors. Then the unknowns are the three coordinates of the receiver, i, and the receiver clock error. The satellite coordinates and the satellite clock error are assumed to be obtained from the navigation message or an other source:

$$P_i^j = \sqrt{(X^j(t) - X_i)^2 + (Y^j(t) - Y_i)^2 + (Z^j(t) - Z_i)^2} + c\delta^j(t) - c\delta_i(t) + \varepsilon \tag{2.5}$$

where the satellite and receiver are represented by j and i, respectively. The satellite clock error $\delta^j(t)$ is known and the Earth-centered and Earth-fixed (ECEF) coordinates X^j, Y^j, Z^j of the satellite can be calculated from given ephemeris data. Therefore, there are 4 unknowns at one epoch; the three ECEF coordinates of the receiver and one receiver clock error. If the observation is repeated n_t times and n_j satellites are viewed, then there are $n_j n_t$ observables and $3+n_t$ unknowns in the static case (fixed receiver coordinates: X_i, Y_i, Z_i). An overdetermined system of equations is obtained if $n_j n_t \geq 3+n_t$. If the receiver is moving, which is the kinematic case, then there are $3n_t + n_t$ unknowns and one must have $n_j n_t \geq 3n_t + n_t = 4n_t$. For the kinematic case, at least 4 satellites must be observed all the time simultaneously.

2.2.2 Relative Positioning

With relative positioning one determines the baseline vector between the known base station and the unknown site. Strictly speaking, one calculates the vector increments because an approximate position is used to linearize the problem. The effect of relative positioning is to eliminate the receiver-dependant or the satellite-dependent errors. The satellite-dependent clock error can be cancelled by the simultaneous observation of the same satellite by two receivers (receiver single-difference). Also, the receiver-dependent clock errors can be cancelled by differencing the single-difference observations of two satellites (double-difference) or just differencing one-way observation of two satellites at one receiver. The satellite- and receiver-dependent but time-independent integer ambiguities can be cancelled by differencing successive-epoch phase data if the satellite is tracked for that time (triple-difference) (Hofmann-Wellenhof et al., 1997).

Single between-receiver difference (from (2.4)):

$$\varphi_{AB}^j(t) = \frac{1}{\lambda}\rho_{AB}^j(t) + N_{AB}^j - f\delta_{AB}(t) + \varepsilon_S \tag{2.6}$$

=> the satellite clock bias has been cancelled

$$\varphi_{AB}^j(t) = \varphi_A^j(t) - \varphi_B^j(t)$$

$$\rho_{AB}^{j}(t) = \rho_{A}^{j}(t) - \rho_{B}^{j}(t)$$
$$= \sqrt{(X^{j}(t-\tau) - X_{A})^{2} + (Y^{j}(t-\tau) - Y_{A})^{2} + (Z^{j}(t-\tau) - Z_{A})^{2}}$$
$$- \sqrt{(X^{j}(t-\tau) - X_{B})^{2} + (Y^{j}(t-\tau) - Y_{B})^{2} + (Z^{j}(t-\tau) - Z_{B})^{2}}$$

$N_{AB}^{j} = N_{A}^{j} - N_{B}^{j}$

$\delta_{AB}(t) = \delta_{A}(t) - \delta_{B}(t)$

ε_S is the noise of the single-differenced observation

t is the GPS time

τ is the signal transmission time

Double-difference:

$$\varphi_{AB}^{jk}(t) = \frac{1}{\lambda}\rho_{AB}^{jk}(t) + N_{AB}^{jk} + \varepsilon_D \tag{2.7}$$

=> the satellite and the receiver clock bias have been cancelled

$\varphi_{AB}^{jk}(t) = \varphi_{AB}^{j}(t) - \varphi_{AB}^{k}(t)$

$\rho_{AB}^{jk}(t) = \rho_{AB}^{j}(t) - \rho_{AB}^{k}(t)$

$N_{AB}^{jk} = N_{AB}^{j} - N_{AB}^{k}$

ε_D is the noise of the double-differenced observation

Triple-difference:

$$\varphi_{AB}^{jk}(t_{12}) = \frac{1}{\lambda}\rho_{AB}^{jk}(t_{12}) + \varepsilon_T \tag{2.8}$$

=> the satellite, the receiver clock bias and the ambiguity have been cancelled

$\varphi_{AB}^{jk}(t_{12}) = \varphi_{AB}^{jk}(t_1) - \varphi_{AB}^{jk}(t_2)$

$\rho_{AB}^{jk}(t_{12}) = \rho_{AB}^{jk}(t_1) - \rho_{AB}^{jk}(t_2)$

ε_T is the noise of the triple-differenced observation

Note that the noises of the single-, double-, and triple-differenced observations such as $\varepsilon_S, \varepsilon_D, \varepsilon_T$ are amplified according to the covariance propagation or the error propagation law. For example, $\varepsilon_S = \sqrt{2}\varepsilon$, $\varepsilon_D = 2\varepsilon$, and $\varepsilon_T = 2\sqrt{2}\varepsilon$ where ε is the noise of the undifferenced phase observation. When one solves for the coordinates in the above models, (2.6), (2.7) and (2.8), the distance between the satellite and the receiver should be expanded up to the first order Taylor series and one must consider the correlation among corresponding differenced observations.

It is an assumption that the error of the phase measurement has a probability distribution with zero expectation and variance, $\sigma_R^{S\,2}$. The superscript S and subscript R indicate the satellite S and the receiver R, respectively. If two receivers A and B collect the phase observations from the i^{th}, j^{th}, and k^{th} satellites during two epochs, t_1 and t_2, then the observation vector (12×1) of phases and the covariance matrix (12×12) for the phases

follow:

$$\underline{\varphi} = \begin{bmatrix} \varphi_A^i(t_1) & \varphi_A^j(t_1) & \varphi_A^k(t_1) & \varphi_B^i(t_1) & \varphi_B^j(t_1) & \varphi_B^k(t_1) \\ \varphi_A^i(t_2) & \varphi_A^j(t_2) & \varphi_A^k(t_2) & \varphi_B^i(t_2) & \varphi_B^j(t_2) & \varphi_B^k(t_2) \end{bmatrix}^T$$

$$\mathrm{cov}(\underline{\varphi}) = \begin{bmatrix} {\sigma_A^i}^2 & 0 & \cdots & 0 & 0 \\ 0 & {\sigma_A^j}^2 & 0 & \ddots & 0 \\ \vdots & 0 & \ddots & 0 & \vdots \\ 0 & \ddots & 0 & {\sigma_B^j}^2 & 0 \\ 0 & 0 & \cdots & 0 & {\sigma_B^k}^2 \end{bmatrix} \tag{2.9}$$

The measured phase $\varphi_R^S(t)$ is linearly independent or uncorrelated with other measurements from a different satellite, receiver or epoch. Therefore the off-diagonal terms in the covariance matrix are zero and the diagonal terms have different values depending on the satellite and the receiver.

The single-differenced observation vector $\underline{\varphi_S}$ is constructed by applying the differential matrix *SD* on the undifferenced phase observation vector.

$$\underline{\varphi_S} = SD\underline{\varphi} = \begin{bmatrix} \varphi_{AB}^i(t_1) \\ \varphi_{AB}^j(t_1) \\ \varphi_{AB}^k(t_1) \\ \varphi_{AB}^i(t_2) \\ \varphi_{AB}^j(t_2) \\ \varphi_{AB}^k(t_2) \end{bmatrix}, \quad SD = \begin{bmatrix} 1 & 0 & 0 & -1 & 0 & 0 & 0 & 0 & 0 & 0 & 0 & 0 \\ 0 & 1 & 0 & 0 & -1 & 0 & 0 & 0 & 0 & 0 & 0 & 0 \\ 0 & 0 & 1 & 0 & 0 & -1 & 0 & 0 & 0 & 0 & 0 & 0 \\ 0 & 0 & 0 & 0 & 0 & 0 & 1 & 0 & 0 & -1 & 0 & 0 \\ 0 & 0 & 0 & 0 & 0 & 0 & 0 & 1 & 0 & 0 & -1 & 0 \\ 0 & 0 & 0 & 0 & 0 & 0 & 0 & 0 & 1 & 0 & 0 & -1 \end{bmatrix} \tag{2.10}$$

If all variances are assumed to have the same value σ^2, then the covariance matrix of the undifferenced observation vector is just an identity matrix multiplied by σ^2. Now the covariance matrix of the single-differenced observation can be calculated by error propagation:

$$\mathrm{cov}(\underline{\varphi_S}) = \sigma^2 SD \cdot SD^T = 2\sigma^2 I_6 \tag{2.11}$$

where I_6 indicates an identity matrix of dimension 6×6. The covariance matrix is a diagonal matrix, which means that the single-differenced observables are still uncorrelated. The variance of the observables is increased by factor of two.

For the double-differenced observation, a correlation exists between the differenced observables. If one assumes *DD* represents the matrix to produce double-differenced observables $\underline{\varphi_D}$, then the observation vector and the covariance matrix are as

follows.

$$\underline{\varphi_D} = DD\underline{\varphi} = \begin{bmatrix} \varphi_{AB}^{ij}(t_1) \\ \varphi_{AB}^{ik}(t_1) \\ \varphi_{AB}^{ij}(t_2) \\ \varphi_{AB}^{ik}(t_2) \end{bmatrix} \quad , \quad DD = \begin{bmatrix} 1 & -1 & 0 & -1 & 1 & 0 & 0 & 0 & 0 & 0 & 0 & 0 \\ 1 & 0 & -1 & -1 & 0 & 1 & 0 & 0 & 0 & 0 & 0 & 0 \\ 0 & 0 & 0 & 0 & 0 & 0 & 1 & -1 & 0 & -1 & 1 & 0 \\ 0 & 0 & 0 & 0 & 0 & 0 & 1 & 0 & -1 & -1 & 0 & 1 \end{bmatrix} \tag{2.12}$$

$$\mathrm{cov}(\underline{\varphi_D}) = \sigma^2 DD \cdot DD^T = \sigma^2 \begin{bmatrix} 4 & 2 & 0 & 0 \\ 2 & 4 & 0 & 0 \\ 0 & 0 & 4 & 2 \\ 0 & 0 & 2 & 4 \end{bmatrix} \tag{2.13}$$

Because of non-zero off-diagonal terms in the covariance matrix, when one solves this double-difference model, one must consider a weight matrix, which is the scaled inverse of the covariance matrix.

In the case of the triple-difference, the differential matrix *TD* and the covariance matrix can be found as follows in a similar way.

$$\underline{\varphi_T} = TD\underline{\varphi} = \begin{bmatrix} \varphi_{AB}^{ij}(t_{12}) \\ \varphi_{AB}^{ik}(t_{12}) \end{bmatrix} \quad , \; TD = \begin{bmatrix} 1 & -1 & 0 & -1 & 1 & 0 & -1 & 1 & 0 & 1 & -1 & 0 \\ 1 & 0 & -1 & -1 & 0 & 1 & -1 & 0 & 1 & 1 & 0 & -1 \end{bmatrix} \tag{2.14}$$

$$\mathrm{cov}(\underline{\varphi_T}) = \sigma^2 TD \cdot TD^T = \sigma^2 \begin{bmatrix} 8 & 4 \\ 4 & 8 \end{bmatrix} \tag{2.15}$$

Like the double-difference, the triple-difference is correlated between differenced observables.

2.2.3 Dilution of Precision (DOP)

The geometry of the tracked GPS satellites is an important factor to get good positioning results and it can be indicated with the dilution of precision (DOP) factor (Hofmann-Wellenhof et al., 1997). The variances of the estimated positions are determined by the variances of the range observation and the DOPs, which are some combinations of the diagonal elements of the covariance matrix. Now, the Gauss-Markov linear model for observables in terms of the position coordinates and the best estimates are,

$$\underline{y} = A\underline{\xi} + \underline{e} \quad , \quad \underline{e} \sim \left(\underline{0}, \sigma^2 \cdot I\right) \tag{2.16}$$

$$\underline{\hat{\xi}} = (A^T A)^{-1} A^T \underline{y} \tag{2.17}$$

where $\underline{y}$ is the observation vector, A is the design matrix and $\underline{\xi}$ is the vector of unknown

position parameters. The model could be either the absolute or relative positioning model; however, the covariance matrix of double and triple differencing positioning can be no longer the identity matrix. The covariance matrix of the unknown parameters is derived as follows.

$$\mathrm{cov}(\underline{\hat{\xi}}) = (A^T A)^{-1} A^T \cdot \sigma^2 I \cdot A(A^T A)^{-1} = \sigma^2 (A^T A)^{-1} \tag{2.18}$$

If the order of the elements of the unknown parameter vector is the east, the north, and the vertical coordinate in a local coordinate system and the clock error, then the above covariance matrix is

$$\mathrm{cov}(\underline{\hat{\xi}}) = \sigma^2 Q = \sigma^2 \begin{bmatrix} q_{ee} & & & off-diagonal & cofactors \\ & q_{nn} & & & \\ & & q_{uu} & & \\ off-diagonal & cofactors & & q_{tt} & \end{bmatrix} \tag{2.19}$$

Where Q is a cofactor matrix and q_{ee}, q_{nn}, q_{uu}, and q_{tt} are cofactors corresponding to four unknown parameters. This is a symmetric matrix and the following DOPs are defined by these diagonal elements.

$$GDOP = \sqrt{q_{ee}^2 + q_{nn}^2 + q_{uu}^2 + q_{tt}^2} \quad ; \quad \text{Geometrical DOP}$$
$$PDOP = \sqrt{q_{ee}^2 + q_{nn}^2 + q_{uu}^2} \quad ; \quad \text{Positioning DOP}$$
$$HDOP = \sqrt{q_{ee}^2 + q_{nn}^2} \quad ; \quad \text{Horizontal DOP}$$
$$VDOP = \sqrt{q_{uu}^2} \quad ; \quad \text{Vertical DOP}$$
$$TDOP = \sqrt{q_{tt}^2} \quad ; \quad \text{Time DOP} \tag{2.20}$$

The DOPs multiplied by the standard deviation σ of the observables give the standard deviation of the unknown parameter estimates. DOPs affect the accuracy of the positioning or navigation solution and change with respect to the satellite motion. The larger the volume defined by the geometric extent of the satellites and the receivers, the better the precision of the solution and the better-conditioned the normal matrix A^TPA of the linear model. For example, three equally distributed satellites near the horizon and one satellite at the zenith make the best geometry. Even though the lower satellite elevation angles tend to have the greater range errors due to the longer path that the signal travels through the atmosphere, usually the geometry has a larger effect on accuracy than range errors (Parkinson et al. 1996). In practice, a PDOP of 1.72 and a GDOP of 1.83 are very good and the worldwide mean for PDOP is 2.5. In conclusion, the DOP factor is a quantitative measurement of this time-variant and satellite-dependent geometry, which is used to select the best set of satellites among many observed satellites.

2.3 GPS Ranging Errors caused by Atmosphere

The electromagnetic signals interact with the charged particles and neutral atoms or molecules in the atmosphere, so the speed and direction of the signal are changed. This phenomenon is called refraction due to the atmosphere (Kleusberg et al., 1996).

In a dispersive medium such as the ionosphere, the refractive index of radio waves is a function of frequency. Also, the modulation of the signal, the P- or C/A-code, has a different refractive index from that of the carrier phase. Two refractive indices for the modulation and carrier phase are as follows:

$$n_g = 1 + \alpha \frac{N_e}{f^2} = \frac{c}{v_g} \quad , \quad n_\varphi = 1 - \alpha \frac{N_e}{f^2} = \frac{c}{v_\varphi} \tag{2.21}$$

where, n_g and n_φ are refractive indices for the modulation and the phase, respectively. f is the frequency of the signal, N_e is the electron density, c is the speed of the light in vacuum, α is a positive constant and v_g and v_φ are the velocities for the modulation and the phase, respectively. Because the refractive index for the modulation is larger than that of the phase, the modulation velocity is smaller than the phase velocity. GPS code pseudorange observation is affected by the modulation refractive index and the carrier phase observation is affected by the phase refractive index. As a consequence, the carrier phase measurement is measured too short (phase advance) and the code pseudorange is measured too long (code delay) (Young et al., 1985). The amounts of ionospheric advance and delay are the same in the two cases. Typical range error is about 10 m, but depends on the elevation. Because of the frequency dependency, these advances or delays can be eliminated (to first order) by observing pseudorange and phase at two frequencies.

The troposphere is a neutral atmosphere, which means this is a non-dispersive medium for radio waves such as the GPS signals. Therefore, propagation is independent of the frequency. In the troposphere, temperature, pressure and humidity affect the radio wave. The dual frequencies for eliminating the effect of the ionosphere can not be used similarly to eliminate the tropospheric effect. This effect gives the same delays for both code and carrier pseudorange. The error range is about 2.0~2.5 m in the zenith direction and increases mostly with the cosecant of the elevation, yielding about a 20~28 m delay at a 5° elevation (Leick, 1995). Generally, this delay term is divided into dry and wet components and then modeled. About 90% of the tropospheric refraction arises from the dry component and about 10% from the wet component (Janes et al., 1989). Even though the dry component is well modeled by knowing in situ atmospheric measurements, the wet component is much more difficult to model because of the strong variations of the water vapor with respect to time and space (Hofmann-Wellenhof et al., 1997).

3 Algorithm derivation and data processing

3.1 The Observation Equations

The observation equations of the four GPS measurement types are given as follows (Goad and Yang, 1995):

$$\Phi_{r,1}^k(t) = \rho_r^k(t) + c(dt_r(t) - dt^k(t)) + T_r^k(t) - \frac{I_r^k(t)}{f_1^2} + \lambda_1 N_{r,1}^k + \lambda_1[\varphi_r(t_0) - \varphi^k(t_0)]_1 + \varepsilon_{r,1}^k \tag{3.1}$$

$$\Phi_{r,2}^k(t) = \rho_r^k(t) + c(dt_r(t) - dt^k(t)) + T_r^k(t) - \frac{I_r^k(t)}{f_2^2} + \lambda_2 N_{r,2}^k + \lambda_2[\varphi_r(t_0) - \varphi^k(t_0)]_2 + b_{r,1}^k(t) + \varepsilon_{r,2}^k \tag{3.2}$$

$$P_{r,1}^k(t) = \rho_r^k(t) + c(dt_r(t) - dt^k(t)) + T_r^k(t) + \frac{I_r^k(t)}{f_1^2} + b_{r,2}^k(t) + e_{r,1}^k \tag{3.3}$$

$$P_{r,2}^k(t) = \rho_r^k(t) + c(dt_r(t) - dt^k(t)) + T_r^k(t) + \frac{I_r^k(t)}{f_2^2} + b_{r,3}^k(t) + e_{r,2}^k \tag{3.4}$$

Here, the subscript *r* indicates the index for the receiver and the superscript *k* for the satellite. c is the speed of light in vacuum; f_1 and f_2 are the L_1 and L_2 carrier frequencies; λ_1 and λ_2 are the L_1 and L_2 carrier wavelengths; $\Phi_{r,1}^k(t)$, $\Phi_{r,2}^k(t)$, $P_{r,1}^k(t)$, and $P_{r,2}^k(t)$ are the phase range and pseudorange measurements from the satellite k and at the receiver r; $\rho_r^k(t)$ is the geometric distance between the satellite's antenna at the signal transmission time and the receiver's antenna at the signal reception time; $T_r^k(t)$ is the tropospheric delay; $I_r^k(t)/f_{1or2}^2$ is the frequency-dependent ionospheric refraction, which causes an advance in phases and a delay in pseudoranges (Section 2.3 in Chapter 2). $N_{r,1}^k$ and $N_{r,2}^k$ are the ambiguities, which are integers for all tracked satellites when the receiver is turned on and they are constant as long as no loss of the signal lock occurs. The one-way phase observables additionally contain a fixed nonzero initial fractional phase term $\lambda[\varphi_r(t_0) - \varphi^k(t_0)]$ that is part of the receiver- and satellite-generated phase signals. The remaining terms $b_{r,1}^k(t)$, $b_{r,2}^k(t)$, and $b_{r,3}^k(t)$ are the relative interchannel biases between $\Phi_{r,1}^k(t)$ and $\Phi_{r,2}^k(t)$, $P_{r,1}^k(t)$, and $P_{r,2}^k(t)$, respectively. They result from the fact that the L1 and L2 signals travel through different hardware paths inside the receiver as well as the satellite transmitter (Coco, 1991). Therefore, the interchannel biases are dependent on both the satellite and the receiver.

While the level of the phase observation noise, ε, is about a millimeter, that of the P and C/A code noises, e, are much larger depending on the type of the receiver. Generally, P-code noise is about 30 centimeters, and C/A code noise can be a meter or

more. From the above four measurement equations, some combinations are possible for eliminating the nuisance parameters such as the ionospheric refraction, the receiver clock errors, and the ambiguities.

3.2 Ion-free, Wide-lane Combination

As mentioned above, the ionospheric effect depends on the frequency of the signal. Thus, by using the dual frequency signals, it is possible to eliminate the first order ionospheric effect by a combination of phase or code measurements. Because the maximum contributions of the 2nd and 3rd order terms of this effect are about 3 cm and less than 1 cm, respectively (Seeber, 1993), eliminating the first order effect might be enough for most applications. The so-called ion-free, wide-lane signal (86 cm wavelength) can be obtained by first multiplying equations (3.1) and (3.2) or (3.3) and (3.4) by the combination coefficients $f_1^2/\{(f_1+f_2)\cdot c\}\approx 2.95$ and $f_2^2/\{(f_1+f_2)\cdot c\}\approx 1.79$, and then taking the differences between the L1 and L2 measurements. The wide-lane signal is the signal having a longer wavelength than that of the original L1 or L2 signal and can be obtained by differencing L1 and L2 phase measurements. The wide-lane combination is known to be less sensitive to the noises because of its longer wavelength (Hofmann-Wellenhof et al.,1997). We have for the carrier phase:

$$\begin{aligned}\varphi^k_{r,ion-free}(t) &= \frac{f_1}{f_1+f_2}\frac{f_1}{c}\Phi^k_{r,1}(t)-\frac{f_2}{f_1+f_2}\frac{f_2}{c}\Phi^k_{r,2}(t)\\ &= \frac{f_1-f_2}{c}\rho^{*k}_r(t)+(f_1-f_2)\{dt_r(t)-dt^k(t)\}+\left(\frac{f_1}{f_1+f_2}N^{*k}_{r,1}-\frac{f_2}{f_1+f_2}N^{*k}_{r,2}\right)+b^k_{r,pahse}(t)+\varepsilon^k_r\end{aligned} \tag{3.5}$$

and for the pseudo-range phase:

$$\begin{aligned}R^k_{r,ion-free}(t) &= \frac{f_1}{f_1+f_2}\frac{f_1}{c}P^k_{r,1}(t)-\frac{f_2}{f_1+f_2}\frac{f_2}{c}P^k_{r,2}(t)\\ &= \frac{f_1-f_2}{c}\rho^{*k}_r(t)+(f_1-f_2)\{dt_r(t)-dt^k(t)\}+b^k_{r,code}(t)+e^k_r\end{aligned} \tag{3.6}$$

Note that $\rho^{*k}_r(t)$ includes the geometric range $\rho^k_r(t)$ and tropospheric delay $T^k_r(t)$. N^{*k}_r is no longer an integer and consists of the integer ambiguity N^k_r and the fractional phase offset $\lambda[\varphi_r(t_0)-\varphi^k(t_0)]$. The interchannel bias is scaled by the combination coefficients and the magnitude of the noise is decreased by a factor 0.7. The reason for the reduced noise is that two combination coefficients applied to the two phase measurements L1 and L2 are less than one. The factor 0.7 comes from $\sqrt{(f_1/f_1+f_2)^2+(f_2/f_1+f_2)^2}$.

3.3 The Time Differenced Measurements

Assuming the measurements have no cycle slips, the ambiguity will remain constant and this can be eliminated when two independent measurements of the same carrier are differenced with respect to time. Similarly, the interchannel bias term could be eliminated by differencing with respect to time if we assume it to be constant. Let's consider that phase and code measurements are obtained for two consecutive epochs (t_i and t_j) without cycle slip.

$$\varphi^k_{r,ion-free}(t_{i,j}) \equiv \varphi^k_{r,ion-free}(t_i) - \varphi^k_{r,ion-free}(t_j) = \frac{f_1 - f_2}{c}\rho^{*k}_r(t_{i,j}) + (f_1 - f_2)\{dt_r(t_{i,j}) - dt^k(t_{i,j})\} + b^k_{r,phase}(t_{i,j}) + \varepsilon \tag{3.7}$$

$$R^k_{r,ion-free}(t_{i,j}) \equiv R^k_{r,ion-free}(t_i) - R^k_{r,ion-free}(t_j) = \frac{f_1 - f_2}{c}\rho^{*k}_r(t_{i,j}) + (f_1 - f_2)\{dt_r(t_{i,j}) - dt^k(t_{i,j})\} + b^k_{r,code}(t_{i,j}) + e \tag{3.8}$$

where,

$$\rho^{*k}_r(t_{i,j}) \equiv \rho^{*k}_r(t_i) - \rho^{*k}_r(t_j)$$
$$dt(t_{i,j}) \equiv dt(t_i) - dt(t_j)$$
$$b^k_{r,phase}(t_{i,j}) \equiv b^k_{r,phase}(t_i) - b^k_{r,phase}(t_j)$$
$$b^k_{r,code}(t_{i,j}) \equiv b^k_{r,code}(t_i) - b^k_{r,code}(t_j)$$
$$\varepsilon \equiv \varepsilon^k_r(t_i) - \varepsilon^k_r(t_j)$$
$$e \equiv e^k_r(t_i) - e^k_r(t_j)\,.$$

Here, the difference between the two consecutive satellite interchannel biases is assumed to show zero mean ($b^k_{phase}(t_{i,j}) = b^k_{code}(t_{i,j}) = \tilde{0}$). It is a reasonable assumption for its behavior is known to be quite stable from one day to the next (personal communication, Joachim Feltens, European Space Operation Center, ESOC, 1999). Therefore, the above two equations (3.7) and (3.8) are represented by the following.

$$\varphi^k_{r,ion-free}(t_{i,j}) = \frac{f_1 - f_2}{c}\rho^{*k}_r(t_{i,j}) + (f_1 - f_2)\{dt_r(t_{i,j}) - dt^k(t_{i,j})\} + b_{r,phase}(t_{i,j}) + \varepsilon \tag{3.9}$$

$$R^k_{r,ion-free}(t_{i,j}) = \frac{f_1 - f_2}{c}\rho^{*k}_r(t_{i,j}) + (f_1 - f_2)\{dt_r(t_{i,j}) - dt^k(t_{i,j})\} + b_{r,code}(t_{i,j}) + e \tag{3.10}$$

In the equations (3.9) and (3.10), the time-differenced interchannel bias terms are no longer dependant on the satellites because of the above assumption on the difference between the two consecutive satellite interchannel biases.

3.4 The Satellite Differenced Measurements

For one receiver tracking two satellites (k^{th} and l^{th}) simultaneously, satellite single differenced measurements are obtained. This single differencing eliminates the receiver dependent effects such as the receiver clock error $dt_r(t)$, the interchannel biases of the receiver $b_r(t)$, and the non-zero initial phase offset of the receiver $\varphi_r(t_0)$ which was already eliminated in time-differencing. By taking difference of time-differenced ion-free wide lane combinations between k^{th} and l^{th} satellite, the equations (3.11) and (3.12) are obtained.

$$\varphi^{k,l}_{r,ion-free}(t_{i,j}) = \varphi^{k}_{r,ion-free}(t_{i,j}) - \varphi^{l}_{r,ion-free}(t_{i,j}) = \frac{f_1 - f_2}{c}\rho^{*k,l}_{r}(t_{i,j}) - (f_1 - f_2)dt^{k,l}(t_{i,j}) + \varepsilon \quad (3.11)$$

$$R^{k,l}_{r,ion-free}(t_{i,j}) = R^{k}_{r,ion-free}(t_{i,j}) - R^{l}_{r,ion-free}(t_{i,j}) = \frac{f_1 - f_2}{c}\rho^{*k,l}_{r}(t_{i,j}) - (f_1 - f_2)dt^{k,l}(t_{i,j}) + e \quad (3.12)$$

According to the error propagation, the standard deviations of the above measurement noises (ε and e) are amplified by a factor of 2 with respect to those of the original ion-free, wide-lane measurement noises because the measurements are differenced twice, in time and between satellites.

Now, two nuisance parameters, namely the receiver clock error and the ambiguity, no longer exist in the above equation. From IGS globally distributed stations coordinates, $\rho^{*k}_{r}(t_{i,j})$ can be calculated and the measurement $\varphi^{k}_{r,ion-free}(t_{i,j})$ is obtained by observing GPS satellites at these stations. Thus, the only unknown parameter is the single-differenced GPS clock error. Rearranging the equation (3.11) in terms of the unknown quantity $dt^{k}(t_{i,j})$, equation (3.13) is obtained.

$$dt^{k,l}(t_{i,j}) = \frac{1}{c}\rho^{*k,l}_{r}(t_{i,j}) - \frac{1}{(f_1 - f_2)}\varphi^{k,l}_{r,ion-free}(t_{i,j}) + \varepsilon \quad (3.13)$$

Only the phase measurements are used for estimating the satellite clock error because they show a relatively small magnitude of noise (a few millimeters), while code measurements have a few decimeters level of noise.

3.5 The Satellite Clock Error and Absolute Positioning

The time- and satellite-differenced, ion-free, phase combination produces the relative variations of the single differenced satellite clock error with respect to the initial epoch. Suppose that the phase measurements are obtained at an IGS fiducial station for *n* epochs. For epoch t_1 and t_2, the time-differenced clock error, $dt^{k,l}(t_{2,1})$, is estimated from the equation (3.13). Then the clock error for the next epoch t_2, $dt^{k,l}(t_2)$ can be expressed in terms of the initial clock error $dt^{k,l}(t_1)$ as follows:

$$dt^{k,l}(t_2) - dt^{k,l}(t_1) = dt^{k,l}(t_{2,1}) \longrightarrow dt^{k,l}(t_2) = dt^{k,l}(t_1) + dt^{k,l}(t_{2,1}) \tag{3.14}$$

For epoch t_2 and t_3,

$$dt^{k,l}(t_3) - dt^{k,l}(t_2) = dt^{k,l}(t_{3,2}) \longrightarrow dt^{k,l}(t_3) = dt^{k,l}(t_1) + dt^{k,l}(t_{3,2}) + dt^{k,l}(t_{2,1}) \tag{3.15}$$

In general, for nth epoch,

$$dt^{k,l}(t_n) - dt^{k,l}(t_{n-1}) = dt^{k,l}(t_{n,n-1}) \longrightarrow dt^{k,l}(t_n) = dt^{k,l}(t_1) + \sum_{i=2}^{n} dt^{k,l}(t_{i,i-1}) \tag{3.16}$$

Therefore, if the satellite clock error at an initial or an arbitrary epoch is available, the satellite clock errors of all epochs are calculated according to the equation (3.16). However, there is no need to know the initial satellite clock error for absolute positioning, because the initial clock error can be absorbed into the ambiguity term in the absolute positioning procedure.

Assume that the relative satellite clock error is estimated and phase measurements are obtained at the unknown sites, whose coordinates are to be determined. After taking the ion-free, wide-lane combination and calculating single differences between satellites, the measurements are described as follows:

$$\begin{aligned}
&\varphi^{k,l}_{r,ion-free}(t_1) = \frac{f_1 - f_2}{c}\rho^{*k,l}_r(t_1) - (f_1 - f_2)dt^{k,l}(t_1) + N^{*k,l}_w + b^{k,l}_{phase}(t_1) + \varepsilon \\
&\varphi^{k,l}_{r,ion-free}(t_2) = \frac{f_1 - f_2}{c}\rho^{*k,l}_r(t_2) - (f_1 - f_2)dt^{k,l}(t_2) + N^{*k,l}_w + b^{k,l}_{phase}(t_2) + \varepsilon \\
&\cdots \\
&\varphi^{k,l}_{r,ion-free}(t_n) = \frac{f_1 - f_2}{c}\rho^{*k,l}_r(t_n) - (f_1 - f_2)dt^{k,l}(t_n) + N^{*k,l}_w + b^{k,l}_{phase}(t_n) + \varepsilon
\end{aligned} \tag{3.17}$$

By putting the estimated satellite clock errors $dt^{k,l}(t_i)$ into the equation (3.17), we find:

$$\begin{aligned}
&\varphi^{k,l}_{r,ion-free}(t_1) = \frac{f_1 - f_2}{c}\rho^{*k,l}_r(t_1) - (f_1 - f_2)dt^{k,l}(t_1) + N^{*k,l}_w + b^{k,l}_{phase} + \varepsilon \\
&\varphi^{k,l}_{r,ion-free}(t_2) = \frac{f_1 - f_2}{c}\rho^{*k,l}_r(t_2) - (f_1 - f_2)dt^{k,l}(t_{2,1}) - (f_1 - f_2)dt^{k,l}(t_1) + N^{*k,l}_w + b^{k,l}_{phase} + \varepsilon \\
&\cdots \\
&\varphi^{k,l}_{r,ion-free}(t_n) = \frac{f_1 - f_2}{c}\rho^{*k,l}_r(t_n) - (f_1 - f_2)\sum_{i=2}^{n} dt^{k,l}(t_{i,i-1}) - (f_1 - f_2)dt^{k,l}(t_1) + N^{*k,l}_w + b^{k,l}_{phase} + \varepsilon
\end{aligned} \tag{3.18}$$

Now, one can define the new phase ambiguity, $\widetilde{N}^{*k,l}_w$, which includes the ambiguity, $N^{*k,l}_w$, the satellite interchannel bias (assumed constant), and the initial satellite clock

error.

$$\widetilde{N}_w^{*k,l} \equiv N_w^{*k,l} + b_{phase}^{k,l} - (f_1 - f_2)dt^{k,l}(t_1) \tag{3.19}$$

By using this time independent variable (assuming no cycle slip and constant interchannel bias), the equation (3.18) is represented as follows.

$$\begin{aligned}
&\varphi_{r,ion-free}^{k,l}(t_1) - \frac{f_1 - f_2}{c} T_r^{k,l}(t_1) = \frac{f_1 - f_2}{c} \rho_r^{k,l}(t_1) + \widetilde{N}_w^{*k,l} + \varepsilon \\
&\varphi_{r,ion-free}^{k,l}(t_2) + (f_1 - f_2)dt^{k,l}(t_{2,1}) - \frac{f_1 - f_2}{c} T_r^{k,l}(t_2) = \frac{f_1 - f_2}{c} \rho_r^{k,l}(t_2) + \widetilde{N}_w^{*k,l} + \varepsilon \\
&\ldots \\
&\varphi_{r,ion-free}^{k,l}(t_n) + (f_1 - f_2)\sum_{i=2}^{n} dt^{k,l}(t_{i,i-1}) - \frac{f_1 - f_2}{c} T_r^{k,l}(t_n) = \frac{f_1 - f_2}{c} \rho_r^{k,l}(t_n) + \widetilde{N}_w^{*k,l} + \varepsilon
\end{aligned} \tag{3.20}$$

In the above equation (from now on the above equation set is called the fundamental equation set), the unknowns are newly defined ambiguity term $\widetilde{N}_w^{*k,l}$ and the position coordinates of the moving receiver $x_r(t)$, $y_r(t)$, and $z_r(t)$, as contained in the range, $\rho_r^{k,l}(t)$. With the measurement $\varphi_{r,ion-free}^{k,l}(t)$, estimated clock error $dt^{k,l}(t_{i,i-1})$ and modeled tropospheric effect $T_r^{k,l}(t)$, these unknowns can be determined.

Theoretically speaking, the positions and ambiguities can be solved simultaneously. The condition number of the design matrix, however, is very large so the inversion and solution are not reliable. Therefore, for a strong solution the float ambiguity, $\widetilde{N}_w^{*k,l}$ should be determined before solving for the absolute positions. The following section explains how the ambiguities are determined as the first step.

3.6 The Float Ambiguity Search (FAS)

This method is based on finding the best initial position which gives the minimum variations of all satellite pairs' ambiguities $\widetilde{N}_w^{*k,l}$. If the initial position is known, all kinematic positions can be determined as long as no cycle slip occurs, because the known initial position has the same information about the ambiguities. However, the accurate initial position is assumed unknown, although an approximate initial position can be obtained by differential pseudorange measurements. With this approximation, the search space that includes the true initial position is constructed. The quality of the approximation determines the number of the grid points, the size of the search space for the candidates of the initial position and also the calculation time. Let us go back to the fundamental equations (3.20):

$$\varphi_{r,ion-free}^{k,l}(t_1) - \frac{f_1 - f_2}{c} T_r^{k,l}(t_1) = \frac{f_1 - f_2}{c} \rho_r^{k,l}(x_r^c(t_1), y_r^c(t_1), z_r^c(t_1)) + \widetilde{N}_w^{*k,l} + \varepsilon \tag{3.21}$$

where $x_i^c(t_1), y_i^c(t_1), z_i^c(t_1)$ are the coordinates of a specific one that has been selected among the initial position candidates. With this candidate, the next epoch's position is determined by differencing the two phase observations as follows.

$$\begin{aligned}&\varphi^{*k,l}_{r,ion-free}(t_2)+(f_1-f_2)dt^{k,l}(t_{2,1})-\varphi^{*k,l}_{r,ion-free}(t_1)+\frac{f_1-f_2}{c}\rho_r^{k,l}(x_r^c(t_1),y_r^c(t_1),z_r^c(t_1))\\&=\frac{f_1-f_2}{c}\rho_r^{k,l}(x_r^c(t_2),y_r^c(t_2),z_r^c(t_2))+\varepsilon\end{aligned} \tag{3.22}$$

where φ^* includes φ and T. If more than four satellites are tracking simultaneously, the above equation is solved for the position coordinates at epoch t_2. Similarly, the position candidates at all epochs can be calculated as follows.

$$\begin{aligned}&\varphi^{*k,l}_{r,ion-free}(t_3)+(f_1-f_2)dt^{k,l}(t_{3,2})-\varphi^{*k,l}_{r,ion-free}(t_2)+\frac{f_1-f_2}{c}\rho_r^{k,l}(x_r^c(t_2),y_r^c(t_2),z_r^c(t_2))\\&=\frac{f_1-f_2}{c}\rho_r^{k,l}(x_r^c(t_3),y_r^c(t_3),z_r^c(t_3))+\varepsilon\\&\ldots\\&\varphi^{*k,l}_{r,ion-free}(t_n)+(f_1-f_2)dt^{k,l}(t_{n,n-1})-\varphi^{*k,l}_{r,ion-free}(t_{n-1})+\frac{f_1-f_2}{c}\rho_r^{k,l}(x_r^c(t_{n-1}),y_r^c(t_{n-1}),z_r^c(t_{n-1}))\\&=\frac{f_1-f_2}{c}\rho_r^{k,l}(x_r^c(t_n),y_r^c(t_n),z_r^c(t_n))+\varepsilon\end{aligned} \tag{3.23}$$

With the kinematic positions determined in this way, the ambiguities of all satellite pairs are calculated every epoch independently.

$$\begin{aligned}&\widetilde{N}_w^{*k,l}(t_1)=\varphi^{k,l}_{r,ion-free}(t_1)-\frac{f_1-f_2}{c}T_r^{k,l}(t_1)-\frac{f_1-f_2}{c}\rho_r^{k,l}(x_r^c(t_1),y_r^c(t_1),z_r^c(t_1))+\varepsilon\\&\widetilde{N}_w^{*k,l}(t_2)=\varphi^{k,l}_{r,ion-free}(t_2)+(f_1-f_2)dt^{k,l}(t_{2,1})-\frac{f_1-f_2}{c}T_r^{k,l}(t_2)-\frac{f_1-f_2}{c}\rho_r^{k,l}(x_r^c(t_2),y_r^c(t_2),z_r^c(t_2))+\varepsilon\\&\ldots\\&\widetilde{N}_w^{*k,l}(t_n)=\\&\varphi^{k,l}_{r,ion-free}(t_n)+(f_1-f_2)\sum_{j=2}^{n}dt^{k,l}(t_{j,j-1})-\frac{f_1-f_2}{c}T_r^{k,l}(t_n)-\frac{f_1-f_2}{c}\rho_r^{k,l}(x_r^c(t_n),y_r^c(t_n),z_r^c(t_n))+\varepsilon\end{aligned} \tag{3.24}$$

If all systematic and random errors are disregarded and the initial position candidate is close to the true initial position, then the above ambiguities should be approximately identical. Therefore, the best initial position can be determined as the one that gives the minimum variations of the all ambiguities. Several methods such as Mader (1992) exist to find the initial position that satisfies the above minimum condition. In the following paragraph, a new method, adapted from the ambiguity function method by Remondi

(1984,1990a) and Mader (1990), is introduced.

First, the float ambiguities are identified as angles of complex numbers of unit magnitude that are constructed as vectors in the complex plane. That is, they are multiplied by $2\pi i$ and made the argument of the exponential. The factor 2π (rad/cyc) is a selectable constant and specifically ensures that those ambiguity vectors, which vary within one cycle of the wide-lane signal ($\leq 86cm$), are represented in the same complex plane. Ambiguity vectors which vary over many cycles can overlap and may be interpreted as the same vectors, even though they are different and locate in the different planes. In order to avoid this problem, the factor is modifiable for the case of poor initial approximations. For example, a factor, $2\pi/2$ ensures that the ambiguity vectors, which vary within two cycles of the wide-lane signal ($\leq 2\times 86cm$), are represented in the same complex plane. Then from the equation (3.24),

$$\exp\left\{2\pi i\cdot \tilde{N}_w^{*k,l}(t_m)\right\}=\cos\left\{2\pi\tilde{N}_w^{*k,l}(t_m)\right\}+i\sin\left\{2\pi\tilde{N}_w^{*k,l}(t_m)\right\}=$$
$$\exp\left\{2\pi i\cdot\left(\begin{array}{l}\varphi_{r,ion-free}^{k,l}(t_m)+(f_1-f_2)\sum_{j=2}^{n}dt^{k,l}(t_{j,j-1})-\frac{f_1-f_2}{c}T_r^{k,l}(t_m)\\ -\frac{f_1-f_2}{c}\rho_r^{k,l}(x_r^c(t_m),y_r^c(t_m),z_r^c(t_m))+\varepsilon\end{array}\right)\right\} \qquad (3.25)$$
$$\leftarrow m=1,2,\ldots,n$$

In the complex plane, the above exponential is represented as a unit vector and the number of vectors is identical to the number of epochs n, if just one satellite pair is considered. The magnitude of the sum of all vectors should be n, if no error and no noise exist and the initial position candidate is the true position. In real situation, however, the magnitude is less than n, because of the receiver random noise error in the phase observations, the systematic and random errors in satellite clock error estimates, the systematic error due to the un-modeled part of the tropospheric delay and the orbit error, even if the initial position candidate is the true position. Disregarding these random and systematic errors, consider the variation of ambiguities caused by a different initial position alone.

Figure 3.1 shows an example for the float ambiguity search algorithm. In this case, the number of epochs is three and the number of satellite pairs is one, so there are three ambiguity vectors in the complex plane, Figures 3.1(a) and 3.1(c). The initial position in (c) is closer to the true initial position than that in (a). Therefore, the three vectors in the case (c) are closer to each other than those in the case (a). Figure 3.1(b) and 3.1(d) shows the summation of the three ambiguity vectors. As expected, the magnitude of the vector sum in (d), 2.93 inches, is larger than that in (c), 2.70 inches. They indicate the stability of ambiguities at every epoch and the accuracy of the initial position. Finally, the position giving the maximum magnitude of the vector sum is determined as the best initial position.

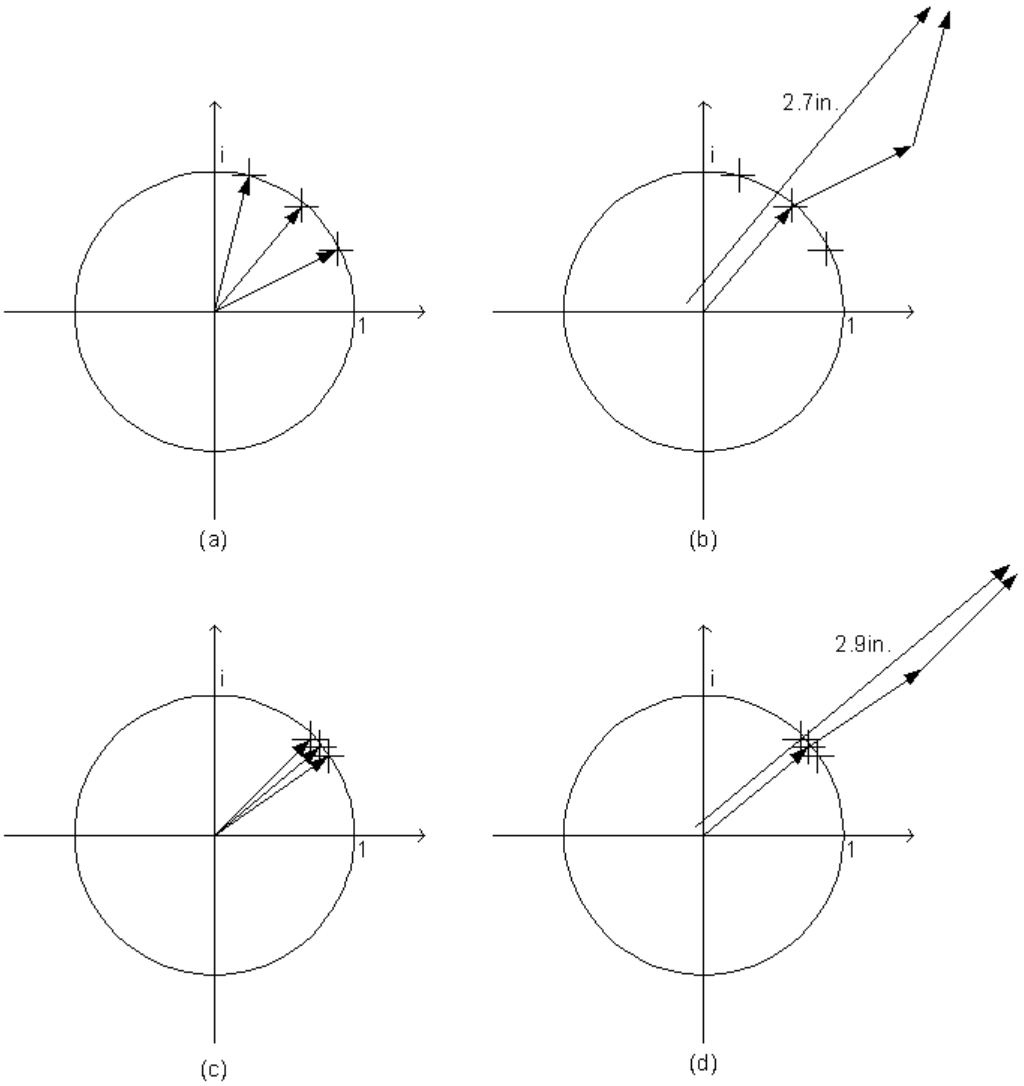

Figure 3.1: An example of the ambiguity vectors in the complex plane.

Figure 3.2 shows ambiguity variations of five satellite pairs calculated by using four different initial positions with real data; (a), (b), (c), and (d). The best initial position is determined after the following steps. First, the ambiguity vectors for all epochs and each satellite pair are summed. Second, the magnitudes of these five vectors sums are combined into one value. This is done for each initial position. Third, the best initial position is determined as the trial position that gives the maximum value. In Figure 3.2, case (d) represents the best initial position. The initial positions in case (a), (b) and (c) are 173 cm, 87 cm and 17 cm apart from the best position, respectively. Finally, the five ambiguities for the five satellite pairs are determined by averaging the ambiguities at all epochs for the best initial position.

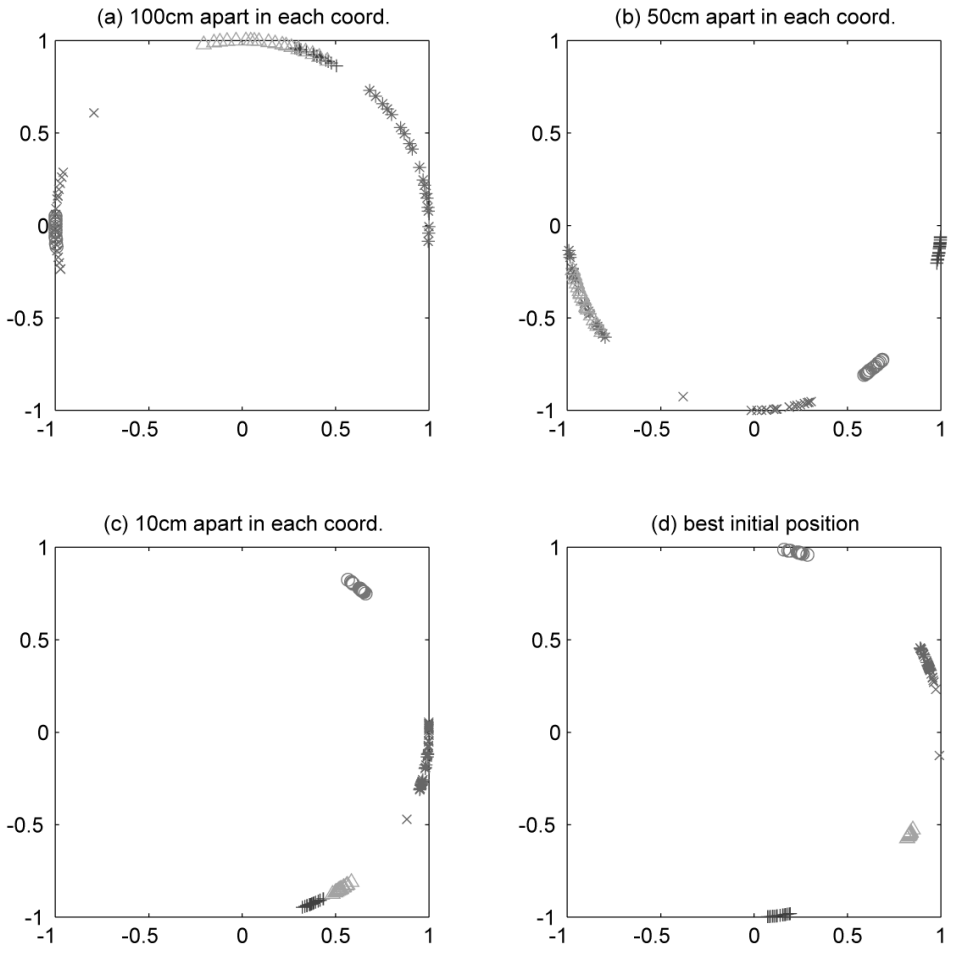

Figure 3.2: Real data example of the ambiguity vectors in the complex plane.

The advantage of this method is that the processing is fast and sequential. In order to calculate variations for a certain time series, one should know the mean value of the data and the data themselves. This means that data must be read twice. The first reading is for calculating the mean value and the second reading is for calculating their variations with respect to the mean, unless the data are stored in memory. Using the above method, however, the minimum variation is found after reading the data only once.

3.6.1 The Coarse-to-Fine Approach for Searching for the Best Initial Position

The critical problem of most searching algorithms is the tremendous number of possible solutions and the long processing time. For example, if there is a $10m \times 10m \times 10m$ cube with a one centimeter grid, then $1001^3 \approx 10^9$ candidates should be tested to find the best initial position. To test all possible initial positions (10^9 candidates) is computationally impractical and even impossible. In the coarse-to-fine approach newly developed in this

research, however, all possible candidates do not need to be checked and the overwhelming computational burden is reduced dramatically.

In order to find the most plausible solution using the coarse-to-fine approach, a search space, having the shape of a cube, is divided into a coarse grid such as one meter. Then the first sub-cell, which shows the maximum value of the sum of all ambiguity vectors, is selected from the search space. From the first sub-cell, the second sub-cell is chosen from among cells in a finer grid according to the condition of the maximum ambiguity vector sum. As a result, the size of the sub-cell (cube) is decreased and the grid interval becomes finer. This process is repeated until the grid interval becomes less than one centimeter. This approach decreases the computational burden dramatically.

For example, if the coarse starting grid interval is one meter in a $10m \times 10m \times 10m$ cube, $11^3 = 1331$ points are tested and the point showing the maximum sum of ambiguity vectors is selected. Then, the first sub-cell, having the selected point at the center of the cell, is constructed with the size $2m \times 2m \times 2m$. Now, the first sub-cell is divided with a 20 cm interval to have the same number of test points as before, 1331. The point with the maximum sum of ambiguity vectors is selected among 1331 candidates and the second sub-cell is constructed as a cube with the size $40cm \times 40cm \times 40cm$ around the selected point. The next grid interval is chosen as 4cm to keep the number of the test points constant, 1331. After repeating the process, the third sub-cell is chosen with a $8cm \times 8cm \times 8cm$ cube. Finally, the grid interval becomes 0.8cm and the size of the fifth sub-cell becomes $1.6cm \times 1.6cm \times 1.6cm$. In the fifth sub-cell, the best initial position is found. In this methodology, only $6655(5 \times 1331)$ points are checked to find out the best solution and the computational burden is reduced from 10^9 to 10^3.

3.7 Least-Squares Adjustment of Parameters

3.7.1 Standard Adjustment

With the satellite clock error estimates and the fixed ambiguities, the fundamental equations (3.20) form a non-linear system with respect to the parameters, that is, the three kinematic coordinates. For an arbitrary epoch *n* and two tracked satellites, the following equation is obtained:

$$l^{k,l}(t_n) := \varphi^{k,l}_{r,ion-free}(t_n) + (f_1 - f_2)\sum_{j=2}^{n} dt^{k,l}(t_{j,j-1}) - \frac{f_1 - f_2}{c} T_r^{k,l}(t_n) - \tilde{N}_w^{*k,l} = \frac{f_1 - f_2}{c} \rho_r^{k,l}(t_n) + \varepsilon \quad (3.26)$$

If one rewrites the last term on the right-hand side explicitly with respect to the parameters, the above equations are described as follows:

$$l^{k,l}(t_n) = \frac{f_1 - f_2}{c} \left\{ \sqrt{\left(x^k(t_n) - x(t_n)\right)^2 + \left(y^k(t_n) - y(t_n)\right)^2 + \left(z^k(t_n) - z(t_n)\right)^2} - \sqrt{\left(x^l(t_n) - x(t_n)\right)^2 + \left(y^l(t_n) - y(t_n)\right)^2 + \left(z^l(t_n) - z(t_n)\right)^2} \right\} + \varepsilon \quad (3.27)$$

where, (x (t_n), y(t_n), z(t_n)) is the position of the receiver at the epoch, t_n, and ($x^k(t_n)$, $y^k(t_n)$, $z^k(t_n)$) and ($x^l(t_n)$, $y^l(t_n)$, $z^l(t_n)$) are the positions for the k^{th} and l^{th} satellites at the epoch, t_n-τ^k and t_n-τ^l, respectively. And, τ is the signal transmission time from the satellite to the receiver and it can be calculated by using the pseudorange observation approximately.

The above equation (3.27) is a non-linear equation with respect to the parameters, x(t_n), y(t_n), and z(t_n). However, a Taylor series expansion truncated after the second order term makes the above non-linear system linear;

$$f(x,y,z) \approx f(x_0,y_0,z_0) + \left.\frac{\partial f(x,y,z)}{\partial x}\right|_0 \Delta x + \left.\frac{\partial f(x,y,z)}{\partial y}\right|_0 \Delta y + \left.\frac{\partial f(x,y,z)}{\partial z}\right|_0 \Delta z \tag{3.28}$$

Applying this to the equation (3.27), the following equation is obtained.

$$\begin{aligned} f^{k,l}(x,y,z) &\equiv \sqrt{\left(x^k-x\right)^2+\left(y^k-y\right)^2+\left(z^k-z\right)^2} - \sqrt{\left(x^l-x\right)^2+\left(y^l-y\right)^2+\left(z^l-z\right)^2} \\ &\approx f_0^{k,l} + \left(\frac{x^l-x_0}{\sqrt{\left(x^l-x_0\right)^2+\left(y^l-y_0\right)^2+\left(z^l-z_0\right)^2}} - \frac{x^k-x_0}{\sqrt{\left(x^k-x_0\right)^2+\left(y^k-y_0\right)^2+\left(z^k-z_0\right)^2}} \right) \cdot \Delta x \\ &\quad + \left(\frac{y^l-y_0}{\sqrt{\left(x^l-x_0\right)^2+\left(y^l-y_0\right)^2+\left(z^l-z_0\right)^2}} - \frac{y^k-y_0}{\sqrt{\left(x^k-x_0\right)^2+\left(y^k-y_0\right)^2+\left(z^k-z_0\right)^2}} \right) \cdot \Delta y \\ &\quad + \left(\frac{z^l-z_0}{\sqrt{\left(x^l-x_0\right)^2+\left(y^l-y_0\right)^2+\left(z^l-z_0\right)^2}} - \frac{z^k-z_0}{\sqrt{\left(x^k-x_0\right)^2+\left(y^k-y_0\right)^2+\left(z^k-z_0\right)^2}} \right) \cdot \Delta z \end{aligned} \tag{3.29}$$

where the dependence on the epoch is omitted to simplify the representation.

The geometrical interpretations of the coefficients are the directional cosine differences with respect to x, y, and z between the l^{th} and the k^{th} satellite. Therefore, the following equation can be represented.

$$f^{k,l}(x,y,z) \approx f_0^{k,l} + \left[C_x^l - C_x^k \quad C_y^l - C_y^k \quad C_z^l - C_z^k \right]_0 \cdot \begin{bmatrix} \Delta x \\ \Delta y \\ \Delta z \end{bmatrix} \tag{3.30}$$

where, the directional cosines are defined by the following.

$$C_x^k = \frac{x^k - x_0}{\sqrt{\left(x^k - x_0\right)^2 + \left(y^k - y_0\right)^2 + \left(z^k - z_0\right)^2}}$$
$$C_y^k = \frac{y^k - y_0}{\sqrt{\left(x^k - x_0\right)^2 + \left(y^k - y_0\right)^2 + \left(z^k - z_0\right)^2}} \tag{3.31}$$
$$C_z^k = \frac{z^k - z_0}{\sqrt{\left(x^k - x_0\right)^2 + \left(y^k - y_0\right)^2 + \left(z^k - z_0\right)^2}}$$

Now, assume that six satellites are tracked. If the satellites are represented as 1, 2, 3, 4, and 5 for five different satellites and "ref" for the reference satellite, which is determined as the satellite showing the maximum elevation, the next equations follow:

$$l^{1,ref}(t_n) \approx l_0^{1,ref} + \frac{f_1 - f_2}{c} \cdot \left[C_x^{ref} - C_x^1 \quad C_y^{ref} - C_y^1 \quad C_z^{ref} - C_z^1\right]_0 \cdot \begin{bmatrix}\Delta x \\ \Delta y \\ \Delta z\end{bmatrix}$$
$$l^{2,ref}(t_n) \approx l_0^{2,ref} + \frac{f_1 - f_2}{c} \cdot \left[C_x^{ref} - C_x^2 \quad C_y^{ref} - C_y^2 \quad C_z^{ref} - C_z^2\right]_0 \cdot \begin{bmatrix}\Delta x \\ \Delta y \\ \Delta z\end{bmatrix}$$
…
$$l^{5,ref}(t_n) \approx l_0^{5,ref} + \frac{f_1 - f_2}{c} \cdot \left[C_x^{ref} - C_x^5 \quad C_y^{ref} - C_y^5 \quad C_z^{ref} - C_z^5\right]_0 \cdot \begin{bmatrix}\Delta x \\ \Delta y \\ \Delta z\end{bmatrix} \tag{3.32}$$

In matrix form:

$$\underline{l} \approx \underline{l}_0 + A \cdot \Delta \underline{x} \quad \text{or} \quad \Delta \underline{l} \approx A \cdot \Delta \underline{x} \tag{3.33}$$

where, vector $\underline{l}$, $\underline{l}_0$, $\Delta\underline{l}$, and $\Delta\underline{x}$ and matrix $\underline{A}$ are defined as follows;

$$\underline{l} \equiv \begin{bmatrix} l^{1,ref}(t) \\ l^{2,ref}(t) \\ l^{3,ref}(t) \\ l^{4,ref}(t) \\ l^{5,ref}(t) \end{bmatrix}, \quad \underline{l}_0 \equiv \begin{bmatrix} l_0^{1,ref}(t) \\ l_0^{2,ref}(t) \\ l_0^{3,ref}(t) \\ l_0^{4,ref}(t) \\ l_0^{5,ref}(t) \end{bmatrix}, \quad \Delta\underline{x} \equiv \begin{bmatrix}\Delta x \\ \Delta y \\ \Delta z\end{bmatrix}, \qquad \Delta\underline{l} \equiv \underline{l} - \underline{l}_0$$

$$A \equiv \frac{f_1 - f_2}{c} \cdot \begin{bmatrix} C_x^{ref} - C_x^1 & C_y^{ref} - C_y^1 & C_z^{ref} - C_z^1 \\ C_x^{ref} - C_x^2 & C_y^{ref} - C_y^2 & C_z^{ref} - C_z^2 \\ C_x^{ref} - C_x^3 & C_y^{ref} - C_y^3 & C_z^{ref} - C_z^3 \\ C_x^{ref} - C_x^4 & C_y^{ref} - C_y^4 & C_z^{ref} - C_z^4 \\ C_x^{ref} - C_x^5 & C_y^{ref} - C_y^5 & C_z^{ref} - C_z^5 \end{bmatrix} \tag{3.34}$$

The solution for the equation (3.33) can be obtained by the condition of the minimum sum of squares of the residuals, $\underline{v}$:

$$\Delta\underline{l} + \underline{v} = A \cdot \Delta\underline{x} \quad \text{with} \quad \underline{v}^T P \underline{v} = \min. \tag{3.35}$$

where, P represents the weight matrix of the model (3.33).

The derivative of the above minimum condition with respect to the parameter vector induces the following normal equation:

$$A^T PA \cdot \Delta\underline{x} = A^T P \cdot \Delta\underline{l} \tag{3.36}$$

The least square solution and its covariance, therefore, are given as follows:

$$\Delta\underline{\hat{x}} = \left(A^T PA\right)^{-1} A^T P \cdot \Delta\underline{l} \quad \text{with} \quad \sum\left(\Delta\underline{\hat{x}}\right) = \left(A^T PA\right)^{-1} \cdot \sigma_0^2 \tag{3.37}$$

where the covariance matrix of the observation is given as $\sum\left(\underline{l}\right) = \sigma_0^2 \cdot P^{-1} = \sigma_0^2 \cdot Q$.

3.7.2 Sequential Adjustment

The Kalman filter provides a recursive solution of the linear discrete data filtering problem (Brown and Hwang, 1997) and it can be applied to update the parameters sequentially. In this sub-section, the static case Kalman gain matrix is derived and it is explained how to update the old estimates by the new observation.

Assume $\underline{\hat{x}}_0$ is the vector of old estimates, $\sum\left(\underline{\hat{x}}_0\right) = \sum_{\mathbf{0}}$ is its covariance matrix, $\underline{l}_1$ is the observation vector, $\sum\left(\underline{l}_1\right) = \sum_{l_1}$ is its covariance matrix, and $\underline{\hat{x}}_1$ is the vector of new estimates. Now, the task to be performed is to use the new observations for improving the old estimates. Let's consider the old estimates as the pseudo-observations and state the following equations:

$$\underline{\hat{x}}_0 + \underline{v}_{x,1} = I \cdot \underline{x}_1 \qquad \ldots \text{ the pseudo-observation equation} \tag{3.38}$$

$$\underline{l}_1 + \underline{v}_{l,1} = A_1 \cdot \underline{x}_1 \qquad \ldots \text{ the observation equation} \tag{3.39}$$

If the above two equations are combined into one equation,

$$\underline{l} + \underline{v} = A \cdot \underline{x}_1 \tag{3.40}$$

where,

$$\underline{l} = \begin{bmatrix} \hat{\underline{x}}_0 \\ \underline{l}_1 \end{bmatrix}, \quad \underline{v} = \begin{bmatrix} \underline{v}_{x,1} \\ \underline{v}_{l,1} \end{bmatrix}, \quad A = \begin{bmatrix} I \\ A_1 \end{bmatrix}$$

The least squares solution of the equation (3.40) is given as the following:

$$\hat{\underline{x}}_1 = \left(A^T \cdot \sum\nolimits^{-1}(\underline{l}) \cdot A\right)^{-1} A^T \cdot \sum\nolimits^{-1}(\underline{l}) \cdot \underline{l} \tag{3.41}$$

where, the weight matrix or the inverse of the covariance matrix is a block diagonal matrix because the old estimates are uncorrelated with the observation.

$$\sum\nolimits^{-1}(\underline{l}) = \begin{bmatrix} \sum_0^{-1} & 0 \\ 0 & \sum_{l,1}^{-1} \end{bmatrix} \tag{3.42}$$

By putting the equation (3.42) into the equation (3.41), the following equation is derived:

$$\hat{\underline{x}}_1 = \left(A_1^T \cdot \sum\nolimits_{l,1}^{-1} A_1 + \sum\nolimits_0^{-1}\right)^{-1} \cdot \left(A_1^T \cdot \sum\nolimits_{l,1}^{-1} \underline{l} + \sum\nolimits_0^{-1} \hat{x}_0\right) \tag{3.43}$$

From the Sherman-Morrison-Woodbury-Schur formula (see Appendix), the equation (3.43) is represented as follows:

$$\hat{\underline{x}}_1 = \left\{\sum\nolimits_0 - \sum\nolimits_0 A_1^T \left(A_1 \sum\nolimits_0 A_1^T + \sum\nolimits_{l,1}\right)^{-1} A_1 \sum\nolimits_0\right\} \cdot \left(A_1^T \cdot \sum\nolimits_{l,1}^{-1} \underline{l} + \sum\nolimits_0^{-1} \hat{x}_0\right) \tag{3.44}$$

Simplifying the equation (3.44), the old estimates and the updates can be divided explicitly.

$$\hat{\underline{x}}_1 = \hat{\underline{x}}_0 + K_1(\underline{l}_1 - A_1 \cdot \hat{\underline{x}}_0) \tag{3.45}$$

where, the Kalman gain matrix is defined as follows:

$$K_1 = \sum\nolimits_0 A_1^T \cdot \left(A_1 \cdot \sum\nolimits_0 A_1^T + \sum\nolimits_{l,1}\right)^{-1} \tag{3.46}$$

The equation (3.45) explains that the new estimates are obtained by adding the old estimates and the updates multiplied by the Kalman gain matrix.

In general, for the $(k-1)^{th}$ estimates and k^{th} observation, the Kalman gain matrix, the new estimates, and its covariance matrix are given as following:

$$
\begin{aligned}
\underline{\hat{x}}_k &= \underline{\hat{x}}_{k-1} + K_k (\underline{l}_k - A_k \cdot \underline{\hat{x}}_{k-1}) \\
K_k &= \Sigma_{k-1} \; A_k^T \cdot \left(A_k \cdot \Sigma_{k-1} \; A_k^T + \Sigma_{l,k} \; \right)^{-1} \\
\Sigma_k &= \left(I - K_k A_k \right) \cdot \Sigma_{k-1}
\end{aligned}
\tag{3.47}
$$

This sequential adjustment algorithm is applied to update the GPS satellite clock error estimates. Actually, the GPS satellite clock error is estimated from some IGS stations, so the same satellite pair's clock error can be estimated from different stations. These redundant estimates are used to update the old estimates with the same weight sequentially. Because the estimates are assumed to have the same weight, the sequential adjustment provides the sequential average of the redundant GPS clock error estimates from different stations. In this case, the design matrix is a vector sum and the number of elements of the design matrix is the same as the number of estimates. The covariance matrix is the identity matrix multiplied by the square of the standard deviation of the clock error estimate, because the estimates are assumed to be independent.

If the estimates are updated one by one, the design matrix is just the scalar number one and the following equations are derived:

$$
\begin{aligned}
\hat{x}_k &= \hat{x}_{k-1} + K_k (x_k - \hat{x}_{k-1}) = \hat{x}_{k-1} + \frac{1}{k+1} (x_k - \hat{x}_{k-1}) \\
K_k &= \sum\nolimits_{k-1} \left(\sum\nolimits_{k-1} \; + \sigma^2 \right)^{-1} = \frac{1}{k+1} \\
\sum\nolimits_k \; &= \left(1 - K_k \right) \cdot \sum\nolimits_{k-1} \; = \frac{1}{k+1} \sigma^2
\end{aligned}
\tag{3.48}
$$

where, $\hat{x}_{k-1}$ is the GPS clock error estimate calculated by using k estimates, x_k is the $(k+1)^{th}$ estimate, and Σ_k is the variance of the estimate, $\hat{x}_k$. Therefore, the final equation gives us the sequential average value every time.

3.8 Data Processing Procedure

3.8.1 GPS Satellite Clock Estimation

The overall procedure of satellite clock estimation is depicted in Figure 3.3. The first step in this algorithm is to calculate the correction derived from a periodic relativistic effect (see Appendix) using the eccentricity, the semi-major axis, and the eccentric anomaly of the GPS satellite orbits, which are updated in the navigation message every 2 hours.

Next, the position of the GPS satellite at the signal emission time is calculated by using the IGS precise orbit and pseudorange observation; and then, the time-differencing of some IGS station observations is performed, where the coordinates of the stations are known. The results of this process, $\left\{ dt_r(t_{i,j}) - dt^k(t_{i,j}) \right\} + \left\{ 1/(f_1 - f_2) \right\} b_{r,phase}(t_{i,j})$ (Eq.

3.9), are the time-differenced GPS satellite clock errors including the receiver clock error and receiver dependent interchannel bias which are not eliminated in this step.

For the GPS satellite position calculation, the orbit's smooth behavior makes interpolation possible within a certain accuracy. According to the studies by Remondi (1989,1991), a 9th-order polynomial interpolator is sufficient for an accuracy of about 10 cm and with a 17th-order interpolator he demonstrated that millimeter-level accuracy can be achieved based on a 40-minute epoch interval. For the tropospheric delay, the modified Hopfield model (Goad and Goodman, 1974) is used.

Finally, after the time- and satellite-differencing, the receiver clock error is eliminated by differencing between satellites. The result of this processing is the time- and satellite-differenced GPS satellite clock error. Redundant values (the same differences of satellite clock errors) can be obtained from other stations and the estimate is obtained by sequentially averaging with equal weights. This assumes that the GPS satellite clock errors estimated using different stations are independent; however, they are not completely uncorrelated since there are slight differences in transmission time for the signal received by stations at the same time. That is, a station on the equator and a station on the pole will receive the GPS signal simultaneously although it was transmitted at slightly different emission times (about 0.02 seconds of difference). It is assumed that the satellite clocks do not significantly vary within this short time period.

3.8.2 Absolute GPS Positioning

Figure 3.4 shows the procedure for estimating the 1 second kinematic GPS positions. All procedures except the float ambiguity search (FAS) step are straightforward and take relatively short processing time. The processing time of FAS depends on the quality of the initial approximate position, i.e., the size of the search space and the grid. The following shows the fundamental equations for position estimation, (3.20):

$$\varphi^{k,l}_{r,ion-free}(t_1) - \frac{f_1 - f_2}{c} T_r^{k,l}(t_1) = \frac{f_1 - f_2}{c} \rho_r^{k,l}(t_1) + \widetilde{N}_w^{*k,l} + \varepsilon$$

$$\varphi^{k,l}_{r,ion-free}(t_2) + (f_1 - f_2) dt^{k,l}(t_{2,1}) - \frac{f_1 - f_2}{c} T_r^{k,l}(t_2) = \frac{f_1 - f_2}{c} \rho_r^{k,l}(t_2) + \widetilde{N}_w^{*k,l} + \varepsilon$$

…

$$\varphi^{k,l}_{r,ion-free}(t_n) + (f_1 - f_2) \sum_{j=2}^{n} dt^{k,l}(t_{j,j-1}) - \frac{f_1 - f_2}{c} T_r^{k,l}(t_n) = \frac{f_1 - f_2}{c} \rho_r^{k,l}(t_n) + \widetilde{N}_w^{*k,l} + \varepsilon$$

As mentioned above, the problem is to calculate the position of the moving receiver $x_r(t)$, $y_r(t)$, and $z_r(t)$ in $\rho_r^{k,l}(t)$ by using the GPS satellite cock error estimates and the fixed float ambiguity.

Now, some abbreviations in Figure 3.4 are explained. "1s IFP", which means one second Ion-Free Phase, is made by combining $\varphi^{k,l}_{r,ion-free}(t_n)$ and $-(f_1 - f_2)/c \cdot T_r^{k,l}(t_n)$ every second. $\varphi^{k,l}_{i,ion-free}(t_n)$ is the ionosphere-free combination of one second GPS

observations. $T_r^{k,l}(t_n)$ is the tropospheric delay term and is modeled with an approximate position. The ion-free phase generator combines these and makes the 'IFP' file. "1s SDCLK", $\sum_{j=2}^{n} dt^{k,l}(t_{j,j-1})$, which means the Satellite Differenced CLocK error (SDCLK), is the interpolated value from 30-second SDCLK which is the result of the processing in the previous Section 3.8.1. A third-degree Lagrange interpolator was used for the interpolation. Next, "1s SDCLK" and "1s IFP" are combined to make "1s OBS". This is the quantity on the left-hand side of the above set of fundamental equations (3.20). Finally, AKGPP (Absolute kinematic GPS precision positioning module) solves the fundamental equations every second by using 1s OBS, one second orbits and the ambiguities provided by FAS.

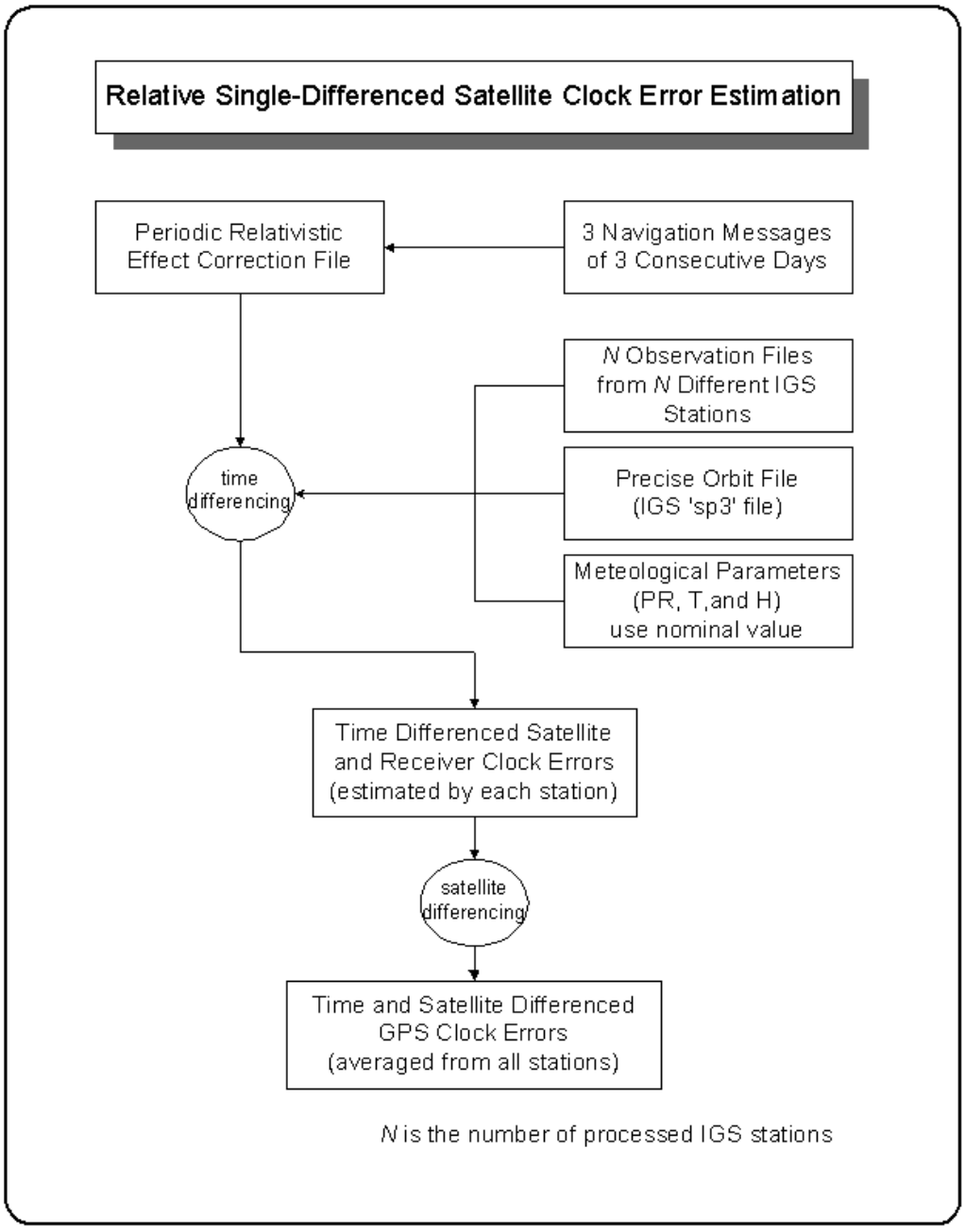

Figure 3.3: Relative Single-differenced Satellite Clock Error Estimation

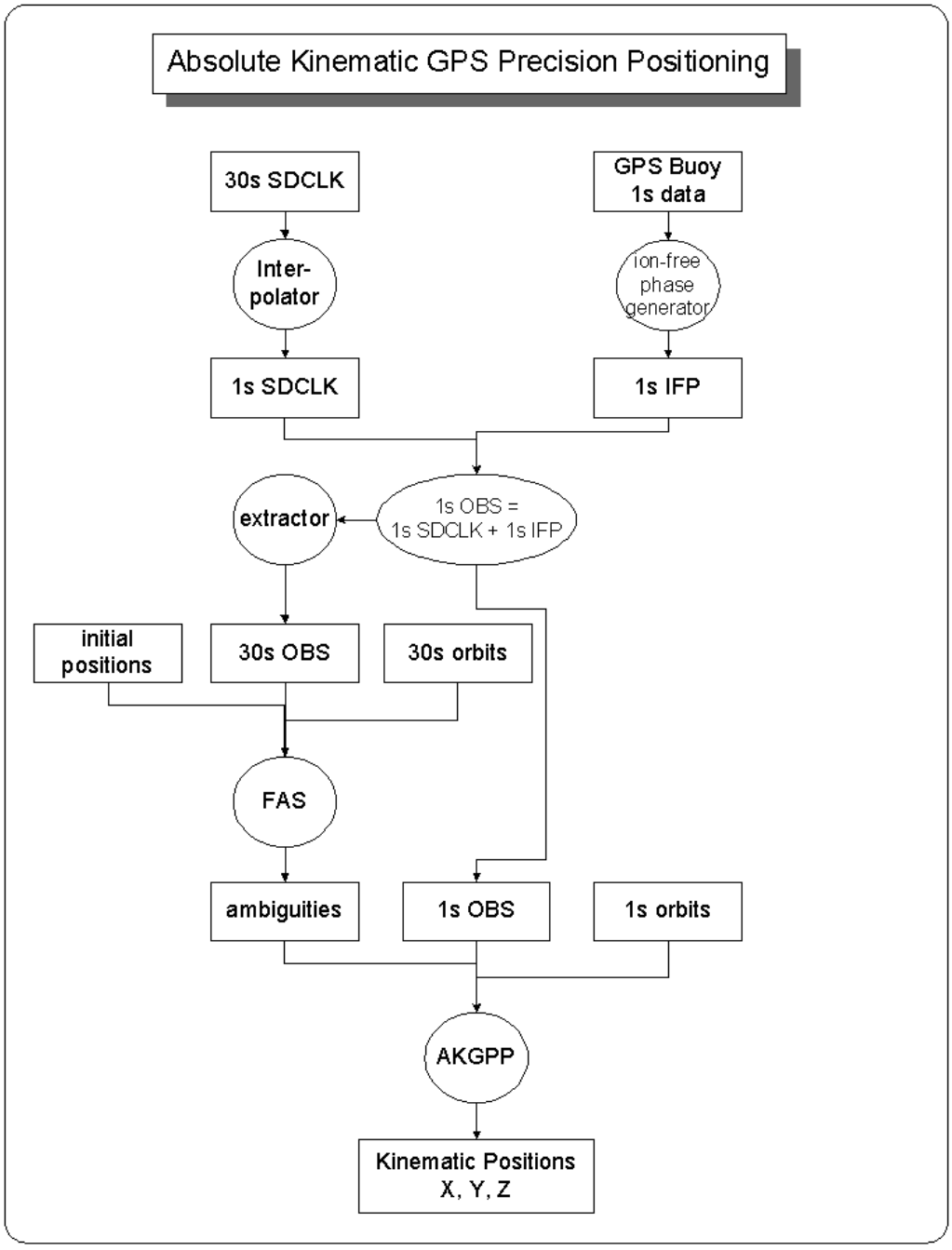

Figure 3.4: Absolute Kinematic GPS Precision Positioning

4 Results and analysis

4.1 Satellite Clock Error Estimates Every 30 Second

Figure 4.1: IGS stations used for clock error estimation

Figure 4.1 shows the distribution of five IGS stations used to estimate the GPS satellite clock errors, as well as the IGS station 'USNA' whose (static) coordinates are to be determined using the absolute positioning algorithm. Naturally, for this test, the coordinates of USNA are assumed known and are used to quantify the errors of estimation. Table 4.1 shows the distance from the five IGS stations to station USNA.

From	To	Length (km)
NLIB	USNA	1214
ALGO	USNA	785
NRC1	USNA	722
WES2	USNA	582
BRMU	USNA	1291

Table 4.1: Baseline Length

In order to generate an orbital ephemeris for each GPS satellite with 30 sec resolution, a 9-th order Lagrange interpolator is applied to the corresponding IGS precise 900-second orbit.

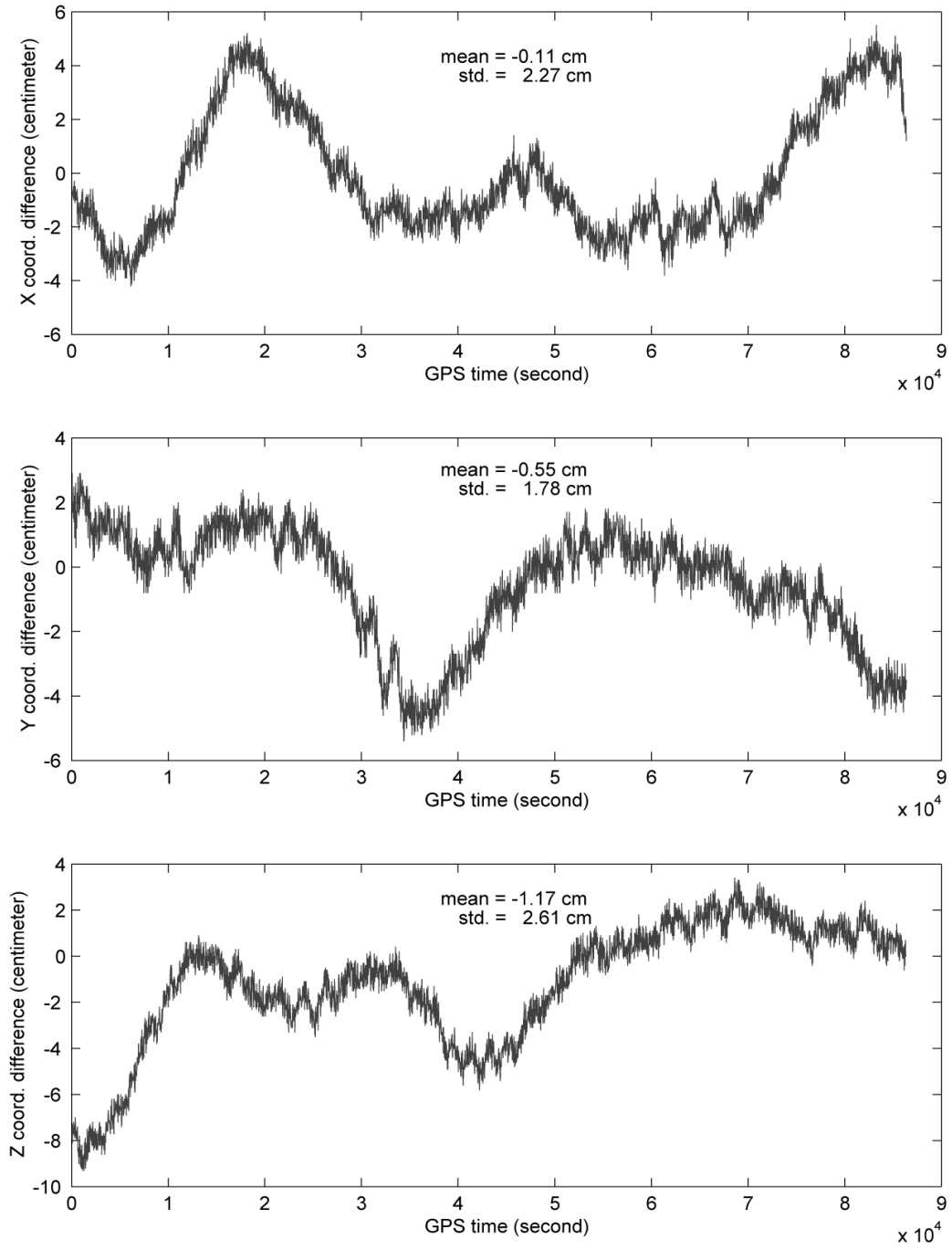

Figure 4.2: Differences between the interpolated IGS orbit and the JPL 30-sec orbit for PRN7

Figure 4.2 represents the difference between the interpolated X, Y, and Z coordinates of the GPS satellite (PRN07) and the JPL 30-second precise orbits (JPL, 1999). Each interpolated coordinate varies from the JPL coordinates with the standard deviation less than 3 cm. The mean differences are on the order of 1 cm or less. From the given standard deviations, we find the standard deviation of range difference to be 3.89 cm, which directly affects the satellite clock error estimation, as seen in (3.13).

Figure 4.3 shows the periodic general relativity effect (see Appendix) with respect to time. Using data from the navigation message provided at 2-hour intervals, 30-second values are calculated by the Lagrange 9th-order interpolator. In case of the PRN4 & PRN7 satellites, the effect increases up to 10 m, while for PRN1 & PRN29 the effect is much smaller, up to 1.5 m. In both cases, this effect is relatively large and the phase or pseudorange measurements should be corrected accurately for precise positioning and clock estimation.

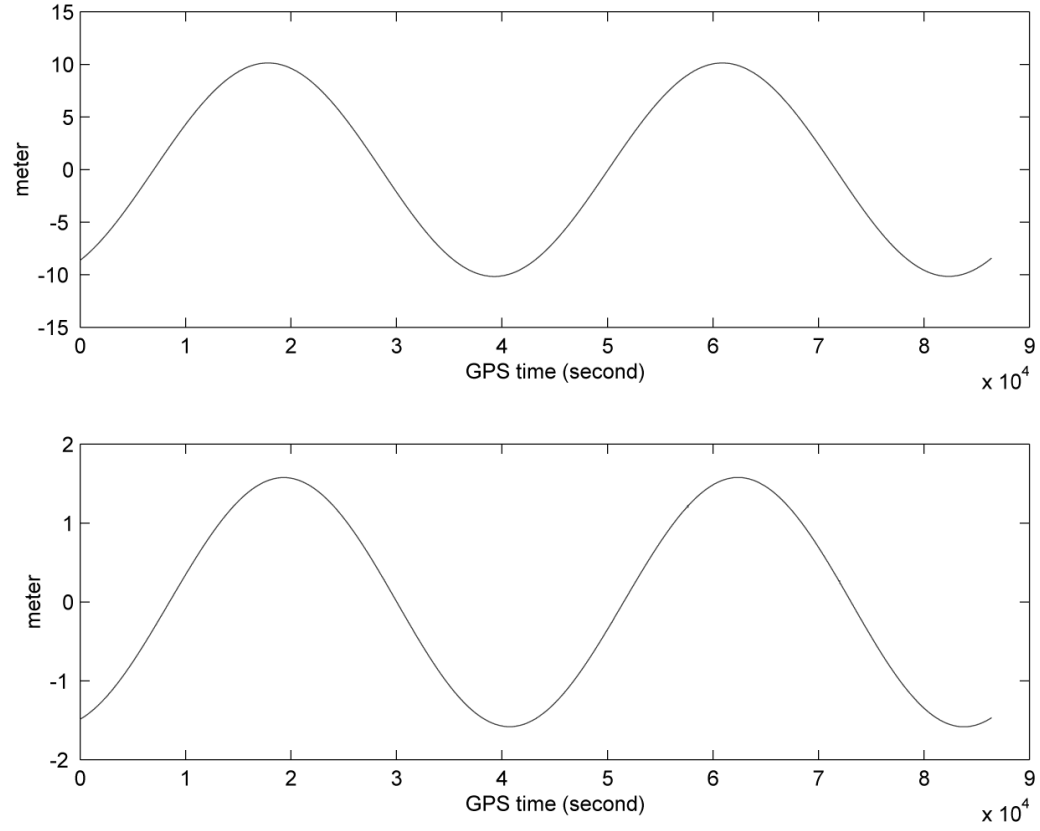

Figure 4.3: Periodic general relativity effect on satellite-differenced range;
PRN4 & PRN7 (top), PRN1 & PRN29 (bottom)

Figure 4.4 shows the time- and satellite-differenced GPS clock error estimates, $dt^{k,l}(t_{i,i-1})$, for the PRN4 & PRN7 satellites, and their differences with respect to the

corresponding estimates from JPL. Analogous results are shown in Figure 4.5 for satellites PRN1 & PRN29. To estimate these clock error differences, observations from five IGS stations are processed independently according to Equation (3.13); and these redundant estimates are then averaged with equal weights sequentially. Figures 4.4 and 4.5 (top portions) indicate that the satellite clock error varies up to ±30 meters at the 30-second resolution, most likely due to Selective Availability (SA). The standard deviations of the estimates with respect to the JPL estimates are less than 1 cm, with mean differences of about 0.1 cm.

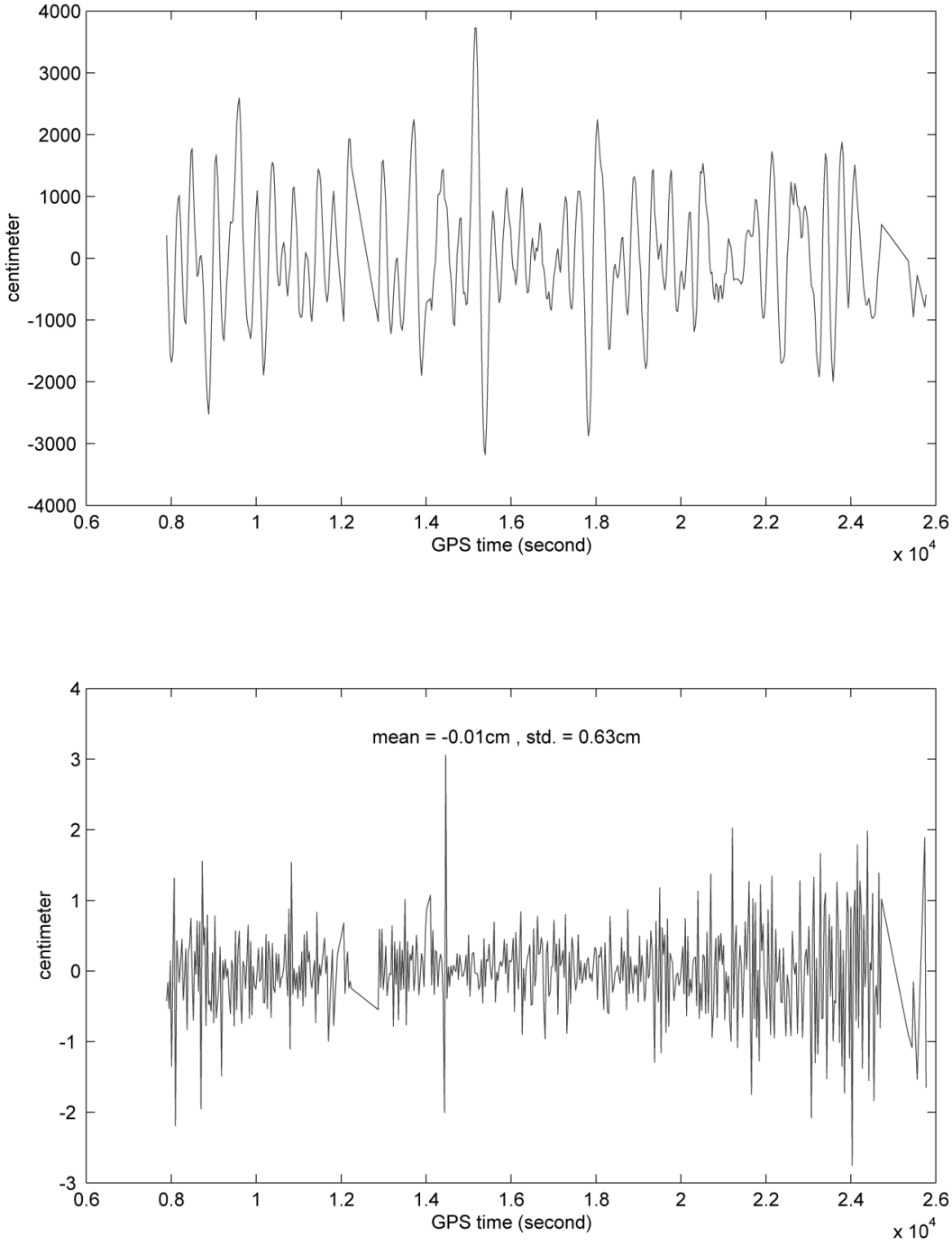

Figure 4.4: Time- and satellite-differenced GPS clock errors (top) and their differences with JPL estimates (bottom) for PRN4 & PRN7

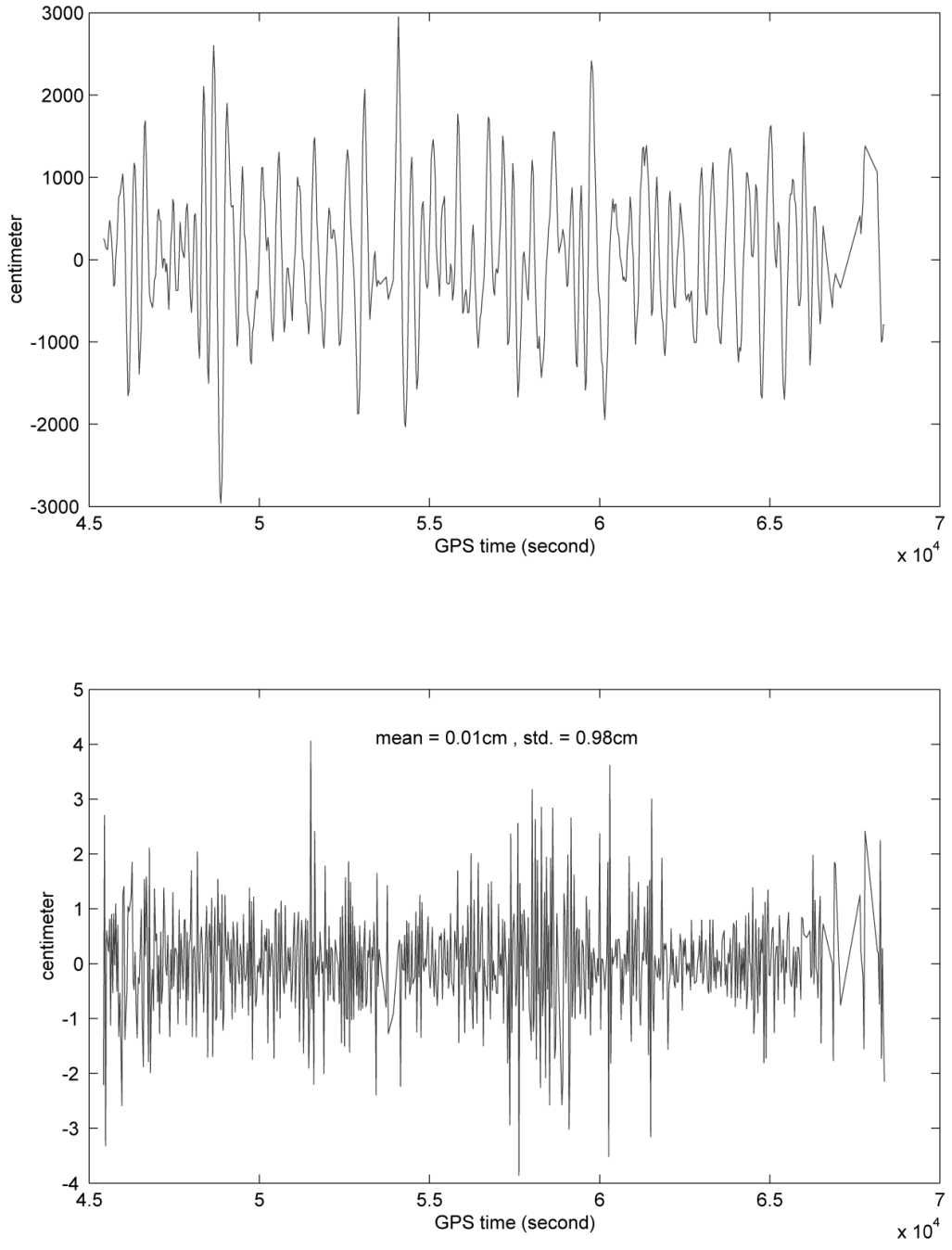

Figure 4.5: Time- and satellite-differenced GPS clock errors (top) and their differences with JPL estimates (bottom) for PRN1 & PRN29

The satellite-differenced GPS clock error estimates, $dt^{k,l}(t_i)$, and their differences with corresponding JPL esitmates are shown in Figure 4.6 for PRN4 & PRN7 and in Figure 4.7 for PRN1 & PRN29. The estimates are calculated by summing the time-differenced estimates according to Equation (3.16) where the initial clock error estimate is obtained from IGS. Again, these results are averages of five independent determinations using five IGS stations. One can see the linear trends in the estimates as well as high frequency fluctuations for both pairs of satellites. These linear trends could also be well determined using the navigation message's clock error information as shown by the straight lines in these plots. The fluctuations in the error, however, cannot de corrected using the navigation message; and the magnitude of the fluctuations is about 200 nanoseconds (60 m). Therefore, one can not avoid an error of ±60 m when performing a clock correction using just the navigation message.

The differences between the clock error estimates in Figure 4.6 and 4.7 and JPL's estimates have standard deviations less than 4 cm, but still contain an offset and other significant systematic components, as shown in the corresponding bottom portions of these figures. JPL's analysis from the global GPS network, called the "Flinn solution" results in satellite position coordinates, clock errors, the receiver coordinates, the receiver clock errors, zenith tropospheric delay and phase biases every 5 minutes. Then all other parameters except the satellite clock errors are interpolated from 5 minutes to 30 second. JPL estimates the satellite clock error every 30 seconds using these interpolated parameters (Jefferson et al., 1996). Their estimates are available via Internet (JPL, 1999).

Some differences in the methods employed by JPL and this research to process the data may explain offsets and systematic variations.

1) Different orbits – Orbits affect the range determination directly, resulting in a difference in the clock error estimation.
2) Modeled tropospheric delay – In our method, the tropospheric delay is not estimated but is modeled, while JPL simultaneously estimates the zenith tropospheric delays with the clock error.
3) Higher order ionospheric effect – the ion-free phase combination used here eliminates only the first-order ionospheric effect, so the higher-order ion effects remain in the error.

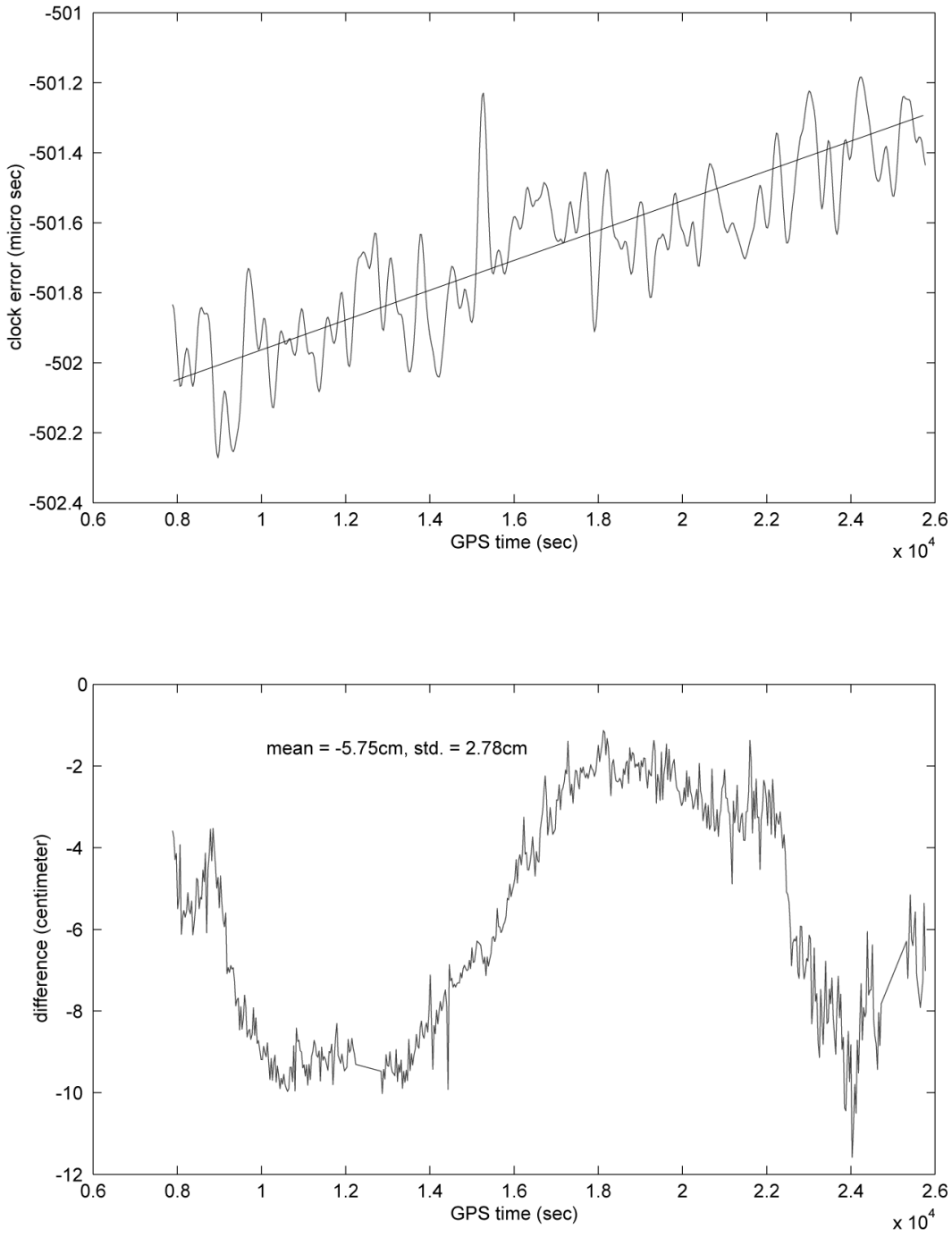

Figure 4.6: Computed satellite-differenced GPS clock errors with linear trend from navigation message (top) and their differences with JPL estimates (bottom) for PRN4 & PRN7

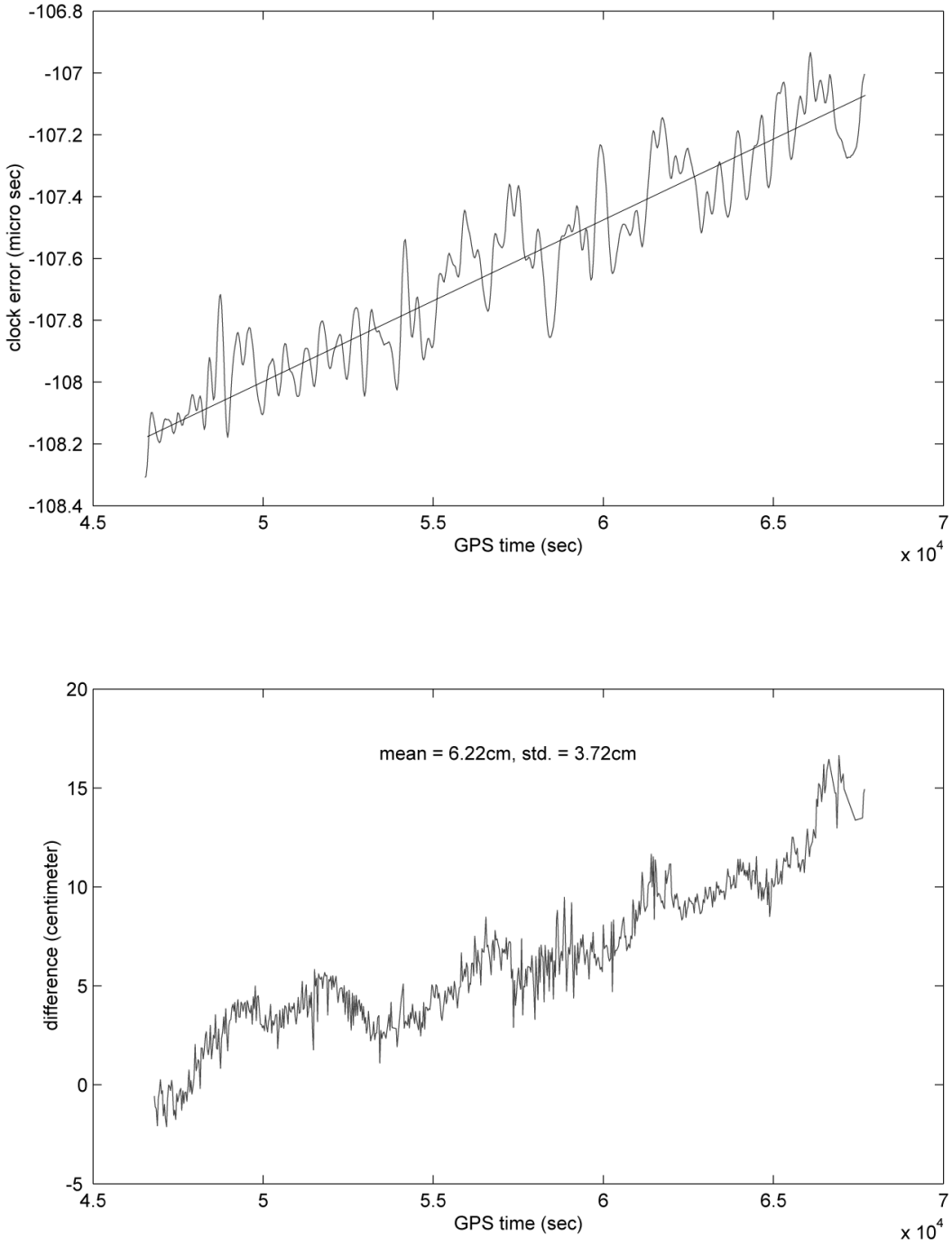

Figure 4.7: Computed satellite-differenced GPS clock errors with linear trend from navigation message (top) and their differences with JPL estimates (bottom) for PRN1 & PRN29

4.2 Absolute Static Positioning Every 30 Second

Using the GPS clock errors thus estimated (using known IGS stations and IGS orbits), precise absolute positioning is possible according to the fundamental Equations (3.20) derived in Chapter 3. One of the IGS stations is selected to check the algorithm in the case of a static receiver. The station USNA is located at various distances (from 600 km to 1300 km) from the five IGS stations used to estimate the GPS clock errors (see Figure 4.1 and Table 4.1). Its coordinates are known (ITRF96) and the clock error estimates determined from the other stations are used to estimate the absolute position of this station. This was done in a two-step process, whereby the float ambiguities, $\widetilde{N}_w^{*k,l}$, were first determined using the float ambiguity search algorithm of Section 3.6. With these fixed, the absolute positions for all epochs were estimated on the basis of the fundamental Equations (3.20).

Figure 4.8 shows the differences between the known (Cartesian) coordinates and the estimated coordinates of the station USNA. The standard deviations are less than 2 cm for a span of 40 minutes of data; for longer periods the standard deviations would increase as more systematic effects enter (as also shown in the lower parts of Figures 4.6 and 4.7). In addition, there are relatively large mean differences up to 18 cm. These may be the result of imperfect ambiguity resolution due to the un-modeled tropospheric delays not already accounted for in the fundamental equations. Absolute positioning requires a good tropospheric delay model.

Using the known coordinates of the station, the ambiguities could be determined directly and much more accurately. In this case, the mean differences of the absolute position errors ranged from 3.4 cm to 6.3 cm and the standard deviations ranged from 1.9 cm to 3.9 cm. The larger standard deviations compared to the previous case are caused by mis-modeled tropospheric delay and other systematic errors in clock error estimates, which are not part of the computed ambiguity. Figure 4.9 shows the static position errors after solving the ambiguities by using the known coordinates at the initial epoch. It indicates that how well the satellite clock errors were estimated for three hours. With the estimates, the static coordinates vary within 4 cm.

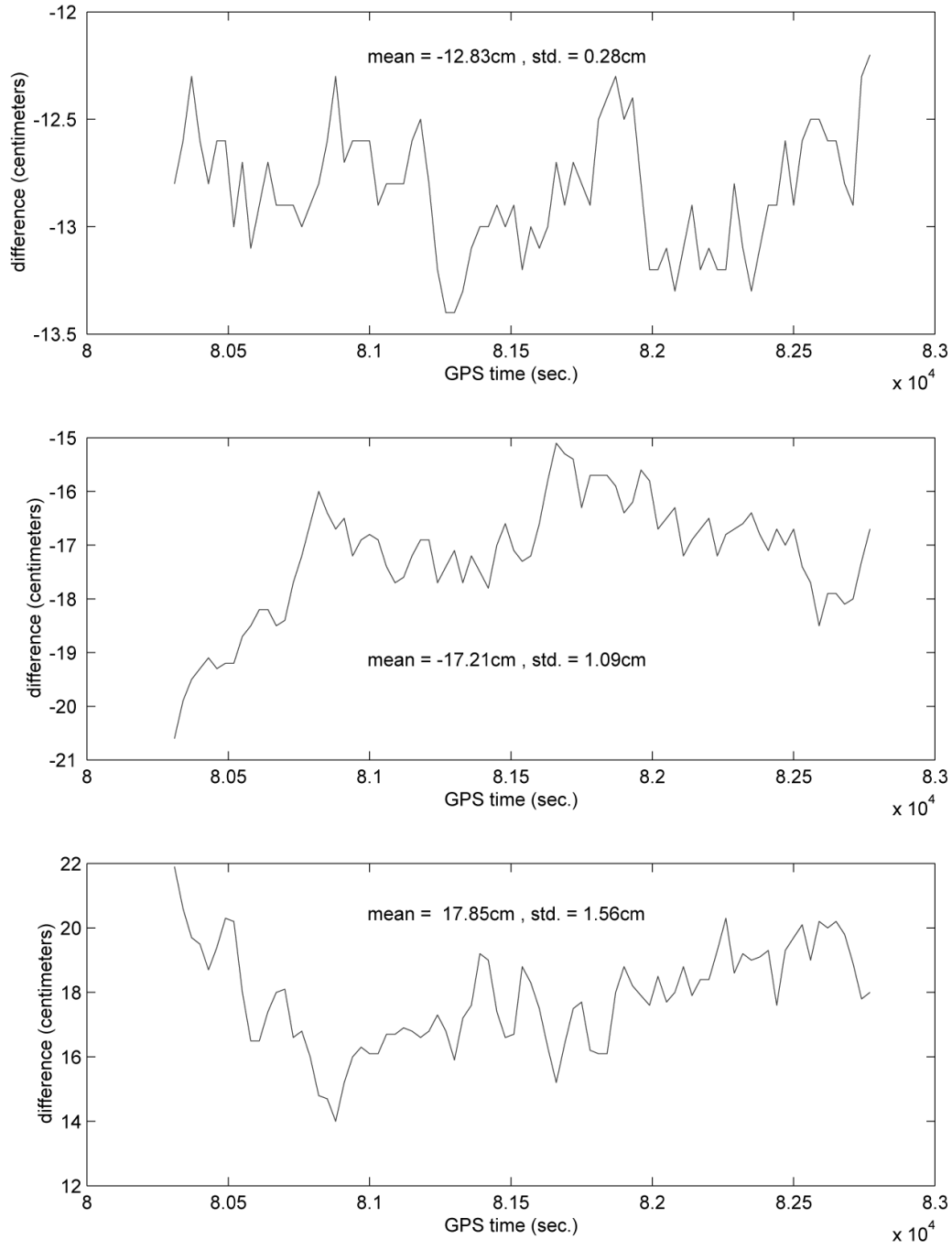

Figure 4.8: Differences between estimated coordinates of USNA and its known coordinates: x(top), y(middle), z(bottom)

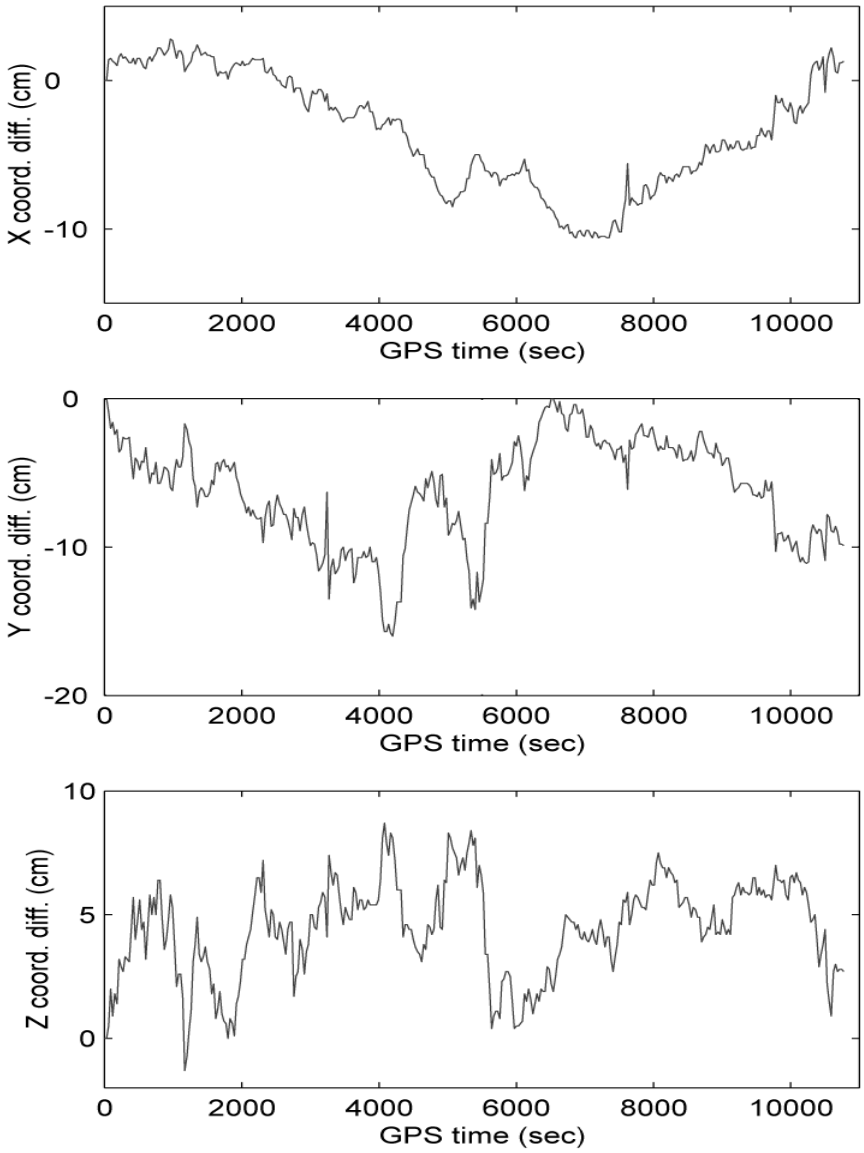

Figure 4.9: Differences between estimated coordinates of USNA and its known coordinates: fixed ambiguity using known coordinates

4.3 Absolute Kinematic Positioning Every 1 Second

4.3.1 GPS Buoy Tests

For the kinematic application, the data from a GPS buoy survey on Lake Michigan (Shum et al., 1999) were processed and compared to the result of the differential GPS (DGPS) solution. Figure 4.10 shows the location of a base station, which is one GPS fiducial site (7031D, NOAA benchmark) chosen for the TOPEX/POSEIDON satellite altimeter

overpass in Lake Michigan, and three IGS stations (NLIB, ALGO, GODE). The GPS buoy was deployed about 350 meters away from the base station and the baseline lengths to NLIB, ALGO, and GODE are 450 km, 740 km, and 890 km, respectively. The data were collected every second at both base station and buoy.

The kinematic DGPS buoy positions were estimated every second by using KARS (Kinematic and Rapid Static Positioning Program) software developed by G. Mader at National Geodetic Survey (NGS) using double-differenced dual-frequency carrier phase data. The positions estimated by KARS were compared with the positions estimated by the absolute positioning algorithm developed for this research.

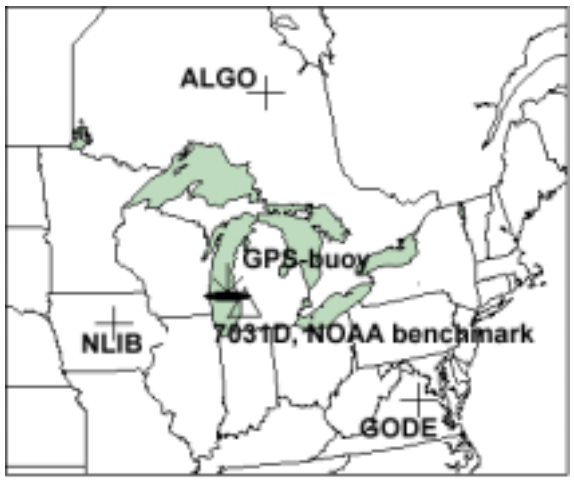

Figure 4.10: Kinematic GPS buoy test area

4.3.2 Interpolation Effect

The satellite clock errors were estimated using the measurements from the 3 IGS stations at every 30 seconds and 1-second clock errors were calculated using a third-degree Lagrange interpolator. After estimating the ambiguities, the buoy's position coordinates were estimated. The only difference in data processing with the static case is the fact that an interpolation was applied to obtain 1-second clock error estimates. This interpolation generates about 8.5 cm RMS interpolation error for the estimates of the satellite clock error originally estimated at 30-second resolution (Zumberge et al., 1998).

Observations collected at 1-second intervals from the receiver established on the NOAA benchmark were used to estimate the satellite-differenced clock error, also at 1-second intervals. Figure 4.11 shows the consistency of these estimates by plotting the differences (crosses) between every 30-th 1-second estimate and the 30-second IGS-based clock error estimates. Also shown (solid line) are the differences between the NOAA benchmark clock error estimates and the interpolated values from the IGS 30-second series at 1-second intervals.

The 30-second GPS clock error estimates from the remote IGS stations are well matched to those from the NOAA station with 1.1 cm standard deviation. The 1-second interpolation errors, however, show short-term fluctuations of relatively large magnitude. The maximum interpolation errors occur in the middle of the 30-second spacing and the standard deviation is about 8.4 cm. This short-term variation is due to SA, specifically the δ-process (dithering the fundamental frequency of the satellite clock). Therefore, one cannot avoid 8-9 cm (s.d.) range error for every satellite or satellite pair when the GPS clock error is interpolated to 1-second resolution from 30-second estimates.

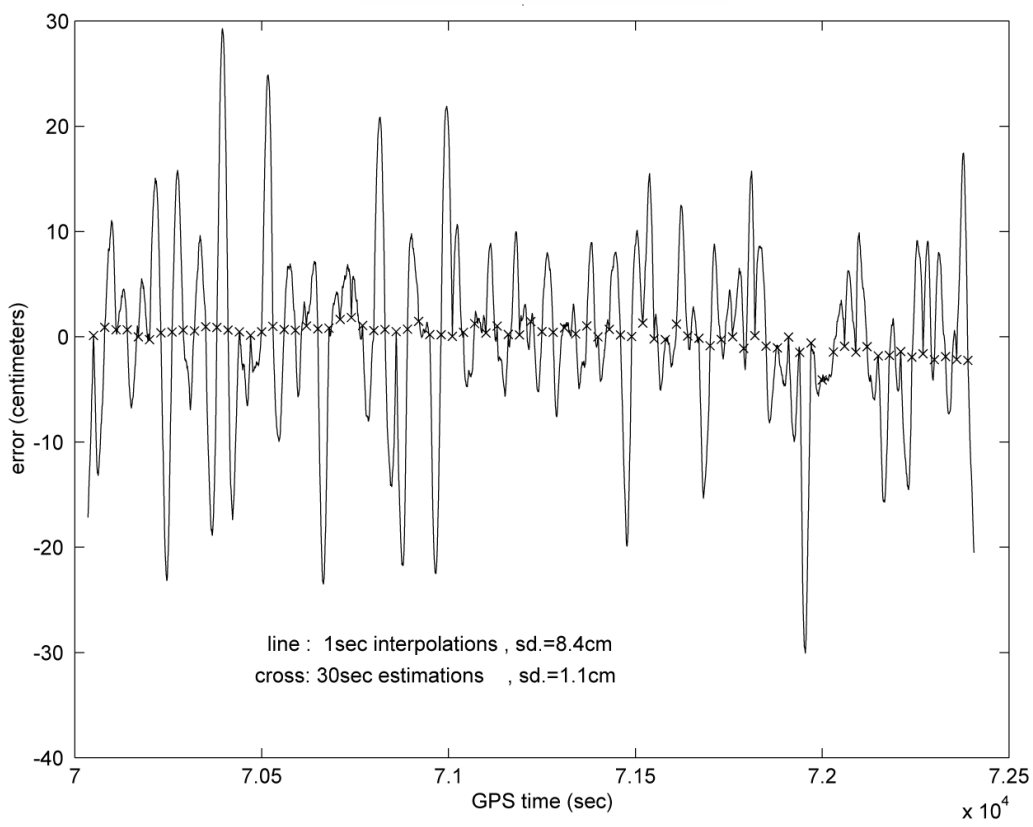

Figure 4.11: GPS clock error interpolation effect (1sec)

The difference between the interpolated clock error and the 1-second estimated clock error has a specific characteristic, which can be analyzed in the frequency domain by using the fast Fourier transformation (FFT). Figure 4.12 shows the frequencies and the corresponding relative amplitudes of the waves consisting of the difference between the interpolated value and the estimated one. Except the pair PRN4/PRN7, all pairs were used to estimate the kinematic positions. The differences for PRN4/PRN7 pair were obtained for different epochs. For every satellite pair, common waves having specific frequencies (0.010, 0.017, and 0.023) can be identified. As mentioned above, these waves mostly came from the δ-process. The interpolator can not provide the

corresponding waves, that is, the interpolated clock error does not have the corresponding variations having certain frequencies such as 0.010, 0.017, and 0.023 cycles/sec. The kinematic positions, furthermore, obtained by using the interpolated clock error will have these additional waves or variations (0.010, 0.017, and 0.023 cycles/sec) due to the interpolation.

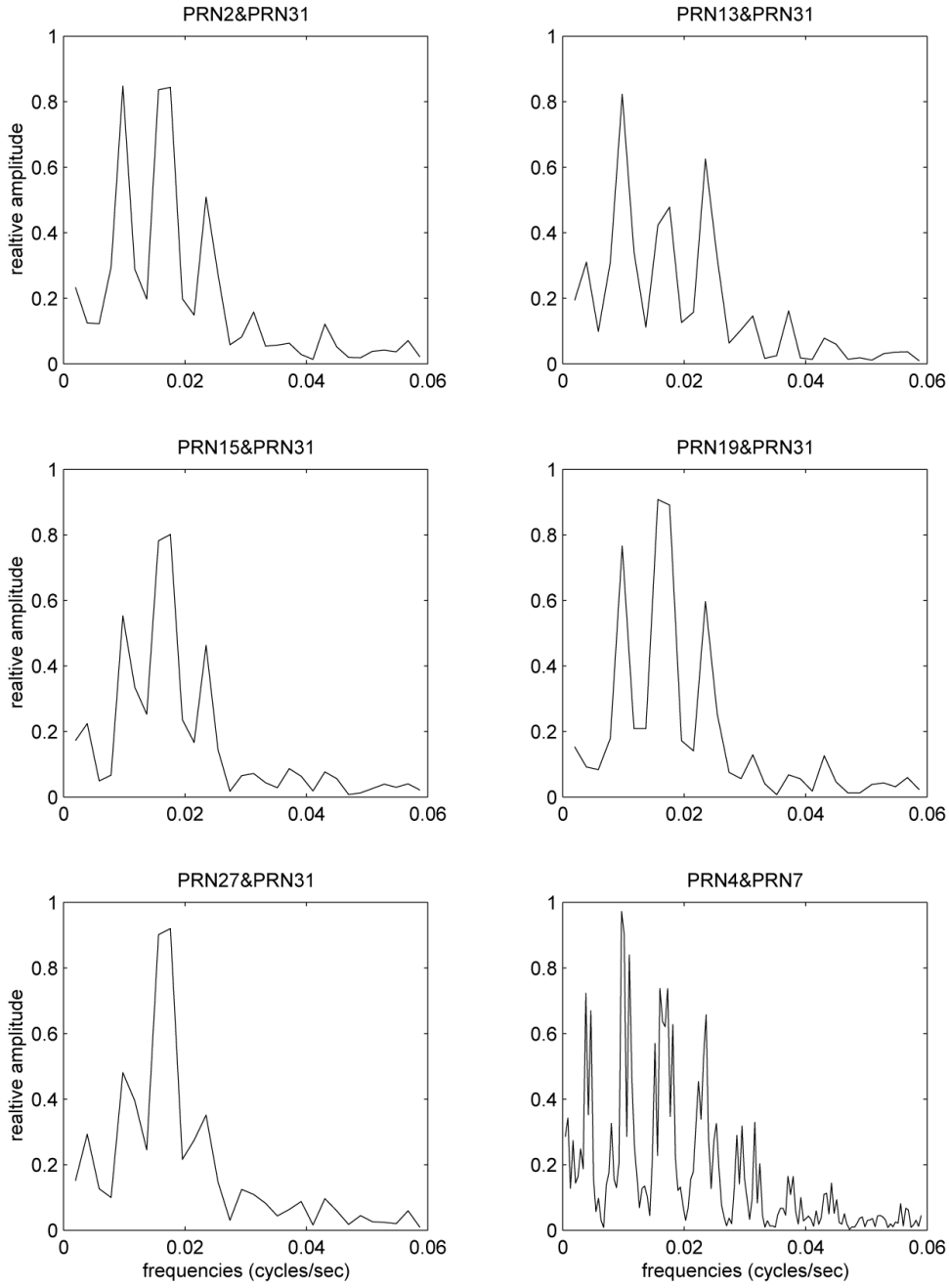

Figure 4.12: Difference between interpolated clock error and estimated one viewed in the frequency domain

4.3.3 One Second Kinematic and Static Positions

The GPS buoy surveying area, in Lake Michigan is located at 42° latitude and -86° longitude. The height estimates, therefore, is much correlated with the Y and Z coordinate estimates. This implies that the estimates of the Y and Z coordinate estimates are less precise than those of the X coordinates, because the geometry constructed by the satellites and the receiver makes the height estimates worse than the horizontal coordinates estimates. At that time, six satellites above 20° elevation were tracked and the respective elevations of the satellites were about 34°, 35°, 27°, 60°, 50°, and 65°. The PDOP (Positioning Dilution Of Precision) was about 3.12, HDOP (Horizontal DOP) was around 1.28, and VDOP (Vertical DOP) was around 2.85.

Figure 4.13 shows a comparison of the kinematic positions estimated by two different methods. The dash lines represent the DGPS positions calculated by the KARS. The solid lines represent the positions calculated by the absolute positioning algorithm with 1-second interpolated satellite clock errors from 30-second estimates. One can see that the general trends are well matched; the differences in each coordinate include biases and high frequency fluctuations. The biases in the X, Y, and Z differences are 20 cm, 39 cm, and 25 cm, and the standard deviations are 7 cm, 23 cm, and 15 cm, respectively. The major error source of the high frequency fluctuation is the interpolation of the clock error to 1-second resolution, as explained above. This conclusion is consistent with static positioning analyses done for the NOAA station (Figure 4.14). Differences between the known coordinates of the base station 7031D and absolute-positioned coordinates using 30-second clock error estimates have standard deviations of (0.5 cm, 2.0 cm, 2.0 cm), while corresponding standard deviations with 1-second interpolated clock error estimates are significantly larger: (5 cm, 21 cm, 15 cm; see Figure 4.14).

As mentioned above in Section 4.3.2, the kinematic positions estimated by using the interpolated clock error show variations having some specific frequencies (0.010, 0.017, and 0.023 cycles/sec). Figure 4.15 shows the amplitudes at all frequencies of the kinematic coordinate solutions. The left three figures represent the case for the absolute positioning solutions and the right three figures for the DGPS solutions. There is no significant difference in the waves of the X coordinate, while there are two additional variations in the Y and Z coordinates within the 0.01 to 0.03 cy/s range. The first dominant one is around 0.017 cy/s, or about 60 s period. The second one is around 0.023 cy/s, or about 40 s period. Evidently, they are due to the interpolation procedure. It is notable that some high frequency fluctuations in the estimated absolute position can be decreased after reducing the amplitude of the corresponding waves in the frequency domain (band-stop filtering). At this moment, however, it should be assumed that the GPS buoy movements do not have motions related to the corresponding periods (60s and 40s).

Figure 4.16 shows the smoothed positions after applying the band-stop filter and reducing the amplitude of the waves came from the interpolation. The ranges of the frequencies of which amplitudes were reduced are from 0.015 to 0.019 and from 0.021 to 0.025 cy/s. The standard deviations of each coordinate were improved after filtering (7cm, 16cm, and 11cm).

There are two applicable explanations for the biases in each coordinate. The first one is the tropospheric delay term. It is known that the absolute positioning requires a good tropospheric delay model. The un-modeled part of the troposphere could yield a similar amount of bias on the kinematic buoy as on the static base station, while it is nicely cancelled out in the case of the short-baseline DGPS. Therefore, the tendency of biases between the kinematic buoy and the static base station is similar as seen in Table 4.2 which shows the magnitude of biases in each coordinate. The un-modeled troposphere can produce these similar biases on both receivers.

	Kinematic buoy	Static base station
dX	20 cm	31 cm
dY	-39 cm	-38 cm
dZ	25 cm	20 cm

Table 4.2: Biases in position estimation

The second possible reason for the bias is the solid Earth tide effect. The nominal coordinates for the base station are the values excluding the tidal effect. In fact, the base station position varies with respect to time because of the periodic solid Earth deformation. The radial component (tidal uplift) of the base station displacement reaches 30 to 40 cm and has to be modeled in the parameter estimation process. The effect is similar for the adjacent stations. For larger station separations, the differential effect has to be considered (Seeber, 1993).

Actually, DGPS doesn't provide the unknown position vector but the baseline vector. In order to get the position vector of the rover, the base station position vector should be known and corrected in terms of tidal site displacement at the corresponding time. The incorrect base station position affects the unknown rover position directly and this effect could appear as biases in the position estimation depending on the period of observation.

It is valuable to compare the baseline vectors solved by both absolute positioning and DGPS because the above two possible causes that induce a bias can be eliminated. In order to calculate the baseline vector in the absolute positioning, the coordinates of the base station should be determined and subtracted from the absolute position vector of the buoy, while DGPS provides the baseline vector directly. Figure 4.17 shows the kinematic buoy position solved by the absolute technique and by DGPS. Biases are reduced to 11cm, 6cm, and 1cm in X, Y, and Z.

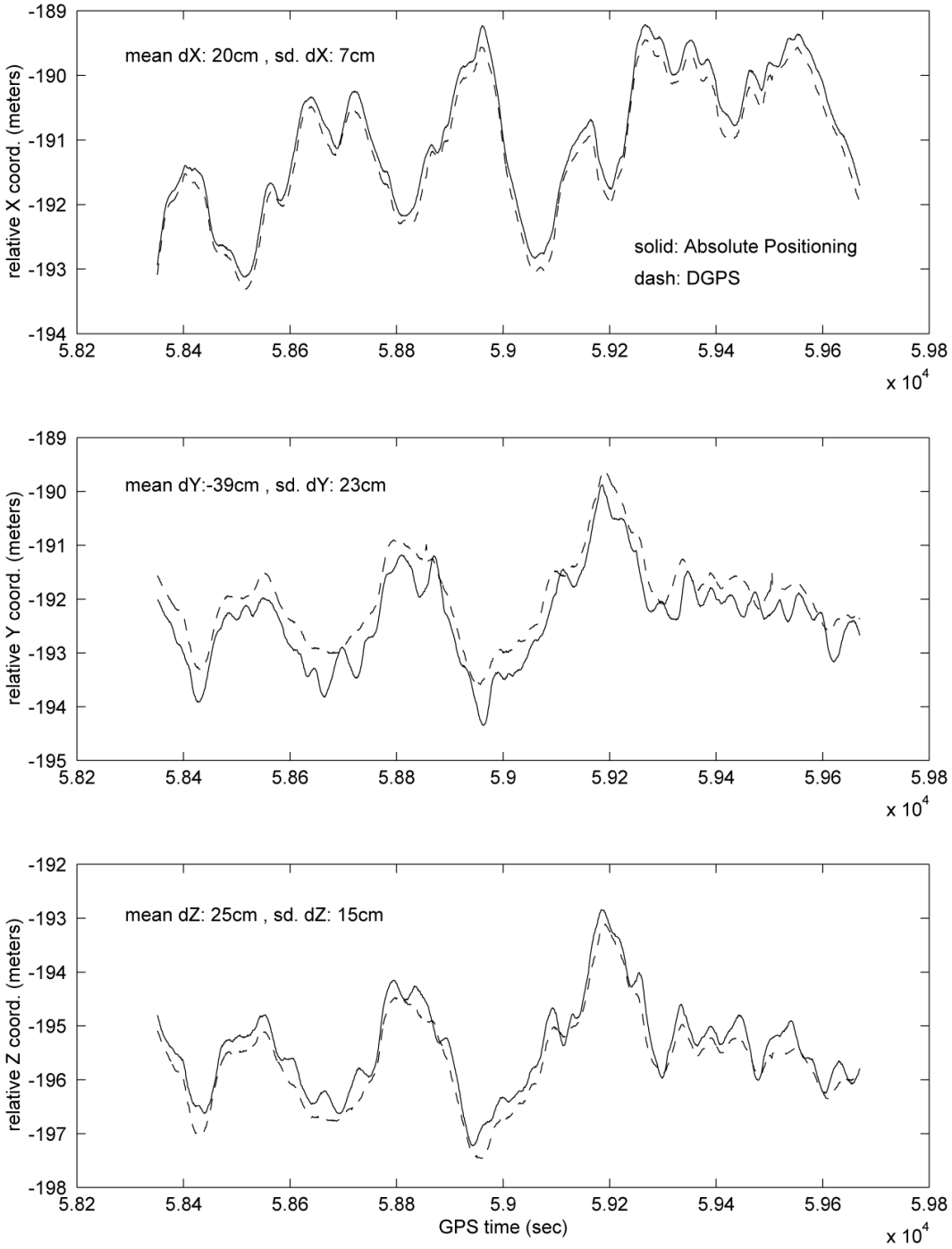

Figure 4.13: Kinematic position comparison

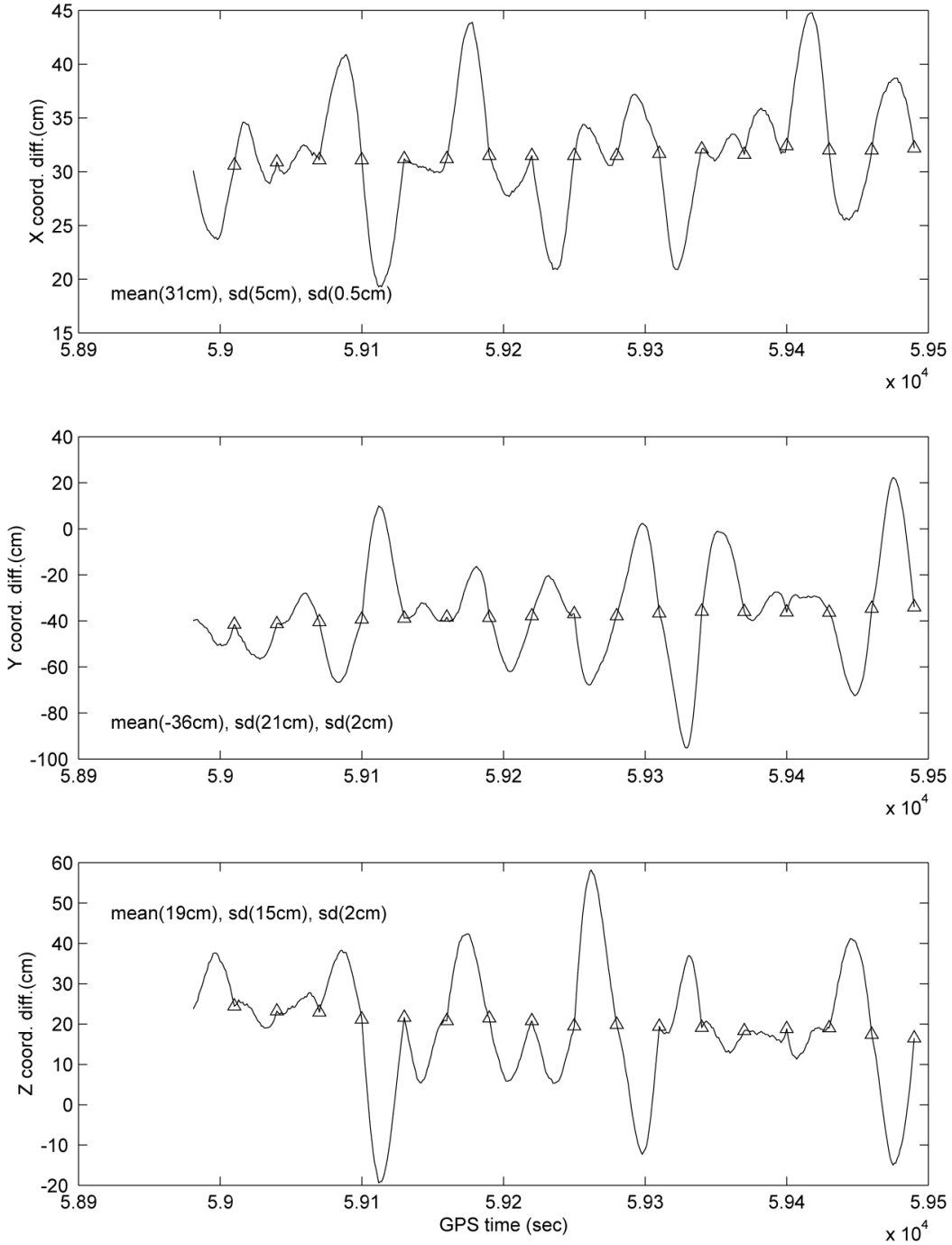

Figure 4.14: Absolute GPS static positioning every 30 second (triangle) and 1 second (line)

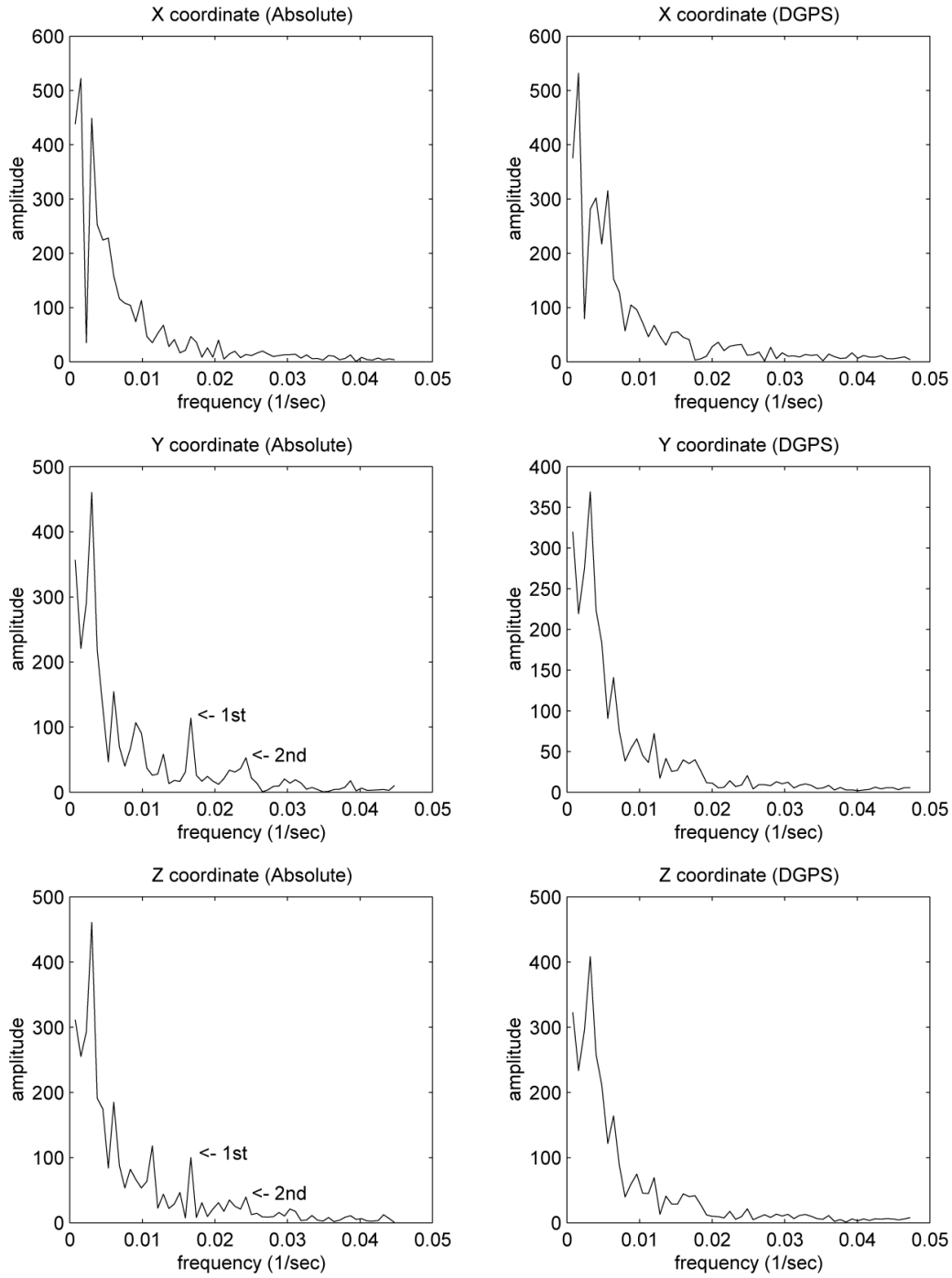

Figure 4.15: Absolute positioning (left) and DGPS results (right) seen in the frequency domain

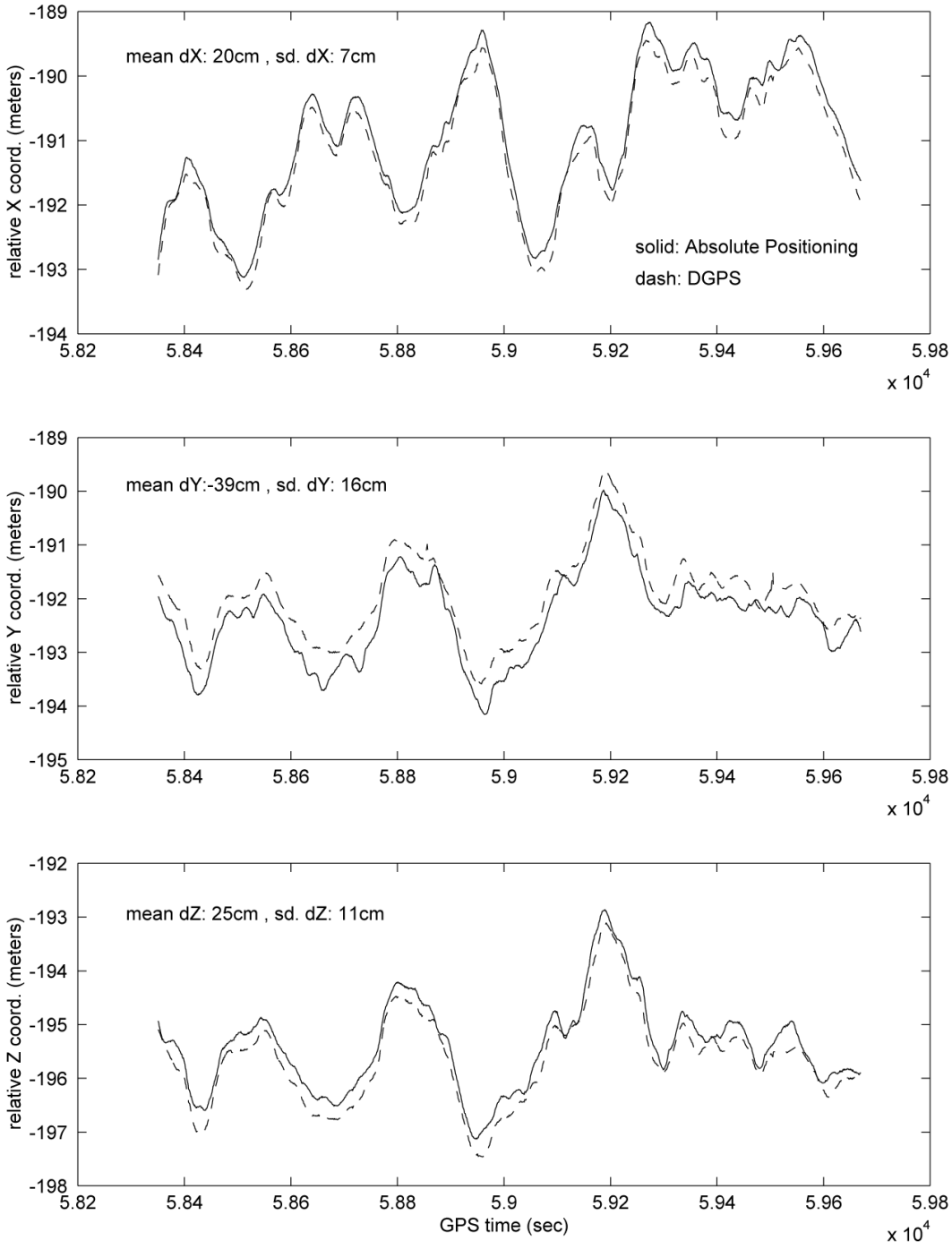

Figure 4.16: GPS buoy kinematic position comparison after applying band-stop filter

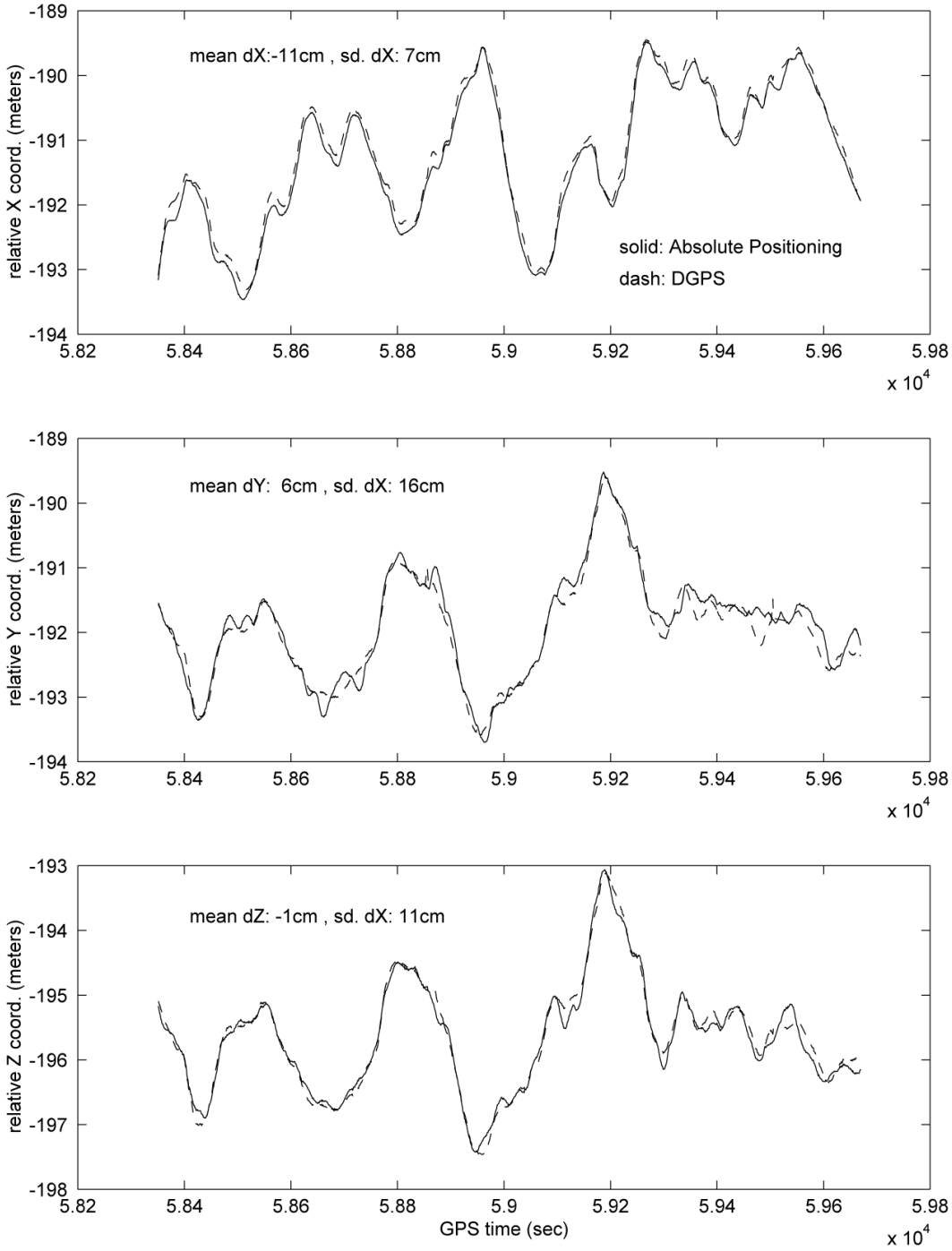

Figure 4.17: GPS buoy kinematic position comparison after applying band-stop filter and using re-estimated base coordinates

5 Conclusion

This study has shown the feasibility to estimate the unknown position with a decimeter level accuracy in an absolute sense (single receiver point positioning). Conventionally, absolute positioning is limited in accuracy due to the satellite clock error associated with selective availability (SA). The accuracy of absolute positioning is several tens of meters without precise satellite clock error estimates. Therefore, the satellite clock error should be estimated precisely before absolute positioning is performed.

The satellite clock error was estimated at a relatively high sampling rate (30 sec) using International GPS Service (IGS) original measurements. Time- and satellite-differenced ion-free, wide-lane phase observables were used for the clock error estimation. Then the initial clock error, inter-channel biases, and the ambiguity were combined into one float ambiguity unknown, which was solved using a newly developed float ambiguity search (FAS) algorithm. The satellite clock error obtained with the above method had standard deviations less than 4 cm in comparison with Jet Propulsion Laboratory (JPL) estimates.

Absolute positioning was performed in the static and kinematic mode with the precisely estimated satellite clock errors. For the static case, it was conducted by estimating one of the IGS fiducial sites where the coordinates were well determined in the international terrestrial reference frame (ITRF). The absolutely estimated position was compared with the known values every 30sec. The position was determined with a precision of 1 cm to 2 cm (continually up to 40 minutes) in all three coordinates. Biases on the order of 18 cm were also detected.

For the applications such as GPS buoy sea level monitoring and aerial photogrammetry, it could be required to estimate the unknown position at a higher rate such as 1 sec. For this purpose, the satellite clock error estimated every 30 sec could be interpolated into the corresponding rate. The interpolation error caused by SA occurs at each satellite and its magnitude is less than 10 cm. In this research, kinematic buoy positions were estimated every 1 sec with the interpolated clock error. The estimated 1 sec kinematic positions showed 7~23 cm precision and 20~40 cm biases in each coordinate. The reason for the worse precision in the 1 sec kinematic positioning than 30 sec positioning is due to the clock interpolation error.

The interpolation could not provide variations at specific frequencies, which came from the δ–process in the selective availability. Therefore, this made the estimated positions fluctuate with the corresponding frequencies. The satellite clock error interpolation effect on the position was reduced after applying a band-stop filter in the frequency domain in an ad hoc empirical strategy to remove the main fluctuations in the δ-process. The band-stop filter increased the precision of the estimates to 7~16 cm.

Biases in both static and kinematic cases could result from the un-modeled part of the tropospheric delay and the solid Earth tide. If so, their effects should be similar at

adjacent sites. In order to prove this supposition, the baseline vectors determined by both absolute positioning and DGPS methods were compared. With this approach, biases were reduced to 1~11 cm.

This research showed that absolute position can be obtained within 10 cm accuracy if the solid Earth tidal correction, a better tropospheric delay model, and the band-stop filter are applied. This accurate absolute positioning can be a powerful technique if the baseline length is too long, if there is no base station near the surveying area, or if the fixed base station's coordinates are not good. Further research is indicated to extend this technique with improved methods to obtain and correct the bias components due to the un-modeled part of tropospheric delay and the solid Earth tidal effect.

APPENDIX

1. Periodic General Relativistic Effect Correction

The general relativistic effect, which is caused by 1) the difference between the gravitational field at the satellite and at the observing site, and 2) the motion of the satellite, is not considered because this effect was corrected in the factory before GPS satellite launch. Another effect arises due to the assumption of a circular orbit. The correction to the range measurement is given by Gibson (1983).

$$\delta_{rel} = \frac{2}{c}\sqrt{GM_E \cdot a} \cdot e \sin E \tag{A.1}$$

where c is the speed of the light in vacuum, e is the eccentricity of the orbital plane, a is the orbital semi major axis, E is the eccentric anomaly of the satellite, and GM_E is the gravitational constant of the Earth.

2. Sherman-Morrison-Woodbury-Schur Formula Derivation

Consider a non-singular matrix M consisting of four block matrices, A, B, C, and D. The diagonal matrices A and D are assumed to be non-singular.

$$M = \begin{bmatrix} A & B \\ m\times m & m\times n \\ C & D \\ n\times m & n\times n \end{bmatrix} \quad \text{for} \quad \exists A^{-1} \text{ and } \exists D^{-1} \tag{A.2}$$

The inverse matrix of M is derived well in Koch (1997).

$$\begin{bmatrix} A & B \\ C & D \end{bmatrix}^{-1} = \begin{bmatrix} A^{-1} + A^{-1}B\left(D - CA^{-1}B\right)^{-1}CA^{-1} & -A^{-1}B\left(D - CA^{-1}B\right)^{-1} \\ -\left(D - CA^{-1}B\right)^{-1}CA^{-1} & \left(D - CA^{-1}B\right)^{-1} \end{bmatrix} \tag{A.3}$$

By multiplying M by a certain matrix, the following matrix becomes a lower-triangular matrix which is easily invertible.

$$\begin{bmatrix} I & -BD^{-1} \\ 0 & I \end{bmatrix} \cdot \begin{bmatrix} A & B \\ C & D \end{bmatrix} = \begin{bmatrix} A - BD^{-1}C & 0 \\ C & D \end{bmatrix} = \begin{bmatrix} T & 0 \\ C & D \end{bmatrix} = L \quad \text{for} \quad T \equiv A - BD^{-1}C \ , \ \exists T^{-1} \tag{A.4}$$

Now the inverse matrix of L is found as follows.

$$\begin{bmatrix} T & 0 \\ C & D \end{bmatrix} \cdot \begin{bmatrix} \alpha & \beta \\ \gamma & \delta \end{bmatrix} = \begin{bmatrix} T\alpha & T\beta \\ C\alpha + D\gamma & C\beta + D\delta \end{bmatrix} = \begin{bmatrix} I & 0 \\ 0 & I \end{bmatrix} \tag{A.5}$$

The solutions for the above equations are:

$$\alpha = T^{-1} \ , \ \beta = 0 \ , \ \gamma = -D^{-1}CT^{-1} \ , \ \delta = D^{-1}$$
$$\therefore L^{-1} = \begin{bmatrix} T^{-1} & 0 \\ -D^{-1}CT^{-1} & D^{-1} \end{bmatrix} \tag{A.6}$$

Using L^{-1} matrix, the inverse matrix of A is found as follows.

$$\begin{bmatrix} T^{-1} & 0 \\ -D^{-1}CT^{-1} & D^{-1} \end{bmatrix} \cdot \begin{bmatrix} I & -BD^{-1} \\ 0 & I \end{bmatrix} \cdot \begin{bmatrix} A & B \\ C & D \end{bmatrix} = I = \begin{bmatrix} A & B \\ C & D \end{bmatrix}^{-1} \cdot \begin{bmatrix} A & B \\ C & D \end{bmatrix} \tag{A.7}$$

$$\therefore \begin{bmatrix} A & B \\ C & D \end{bmatrix}^{-1} = \begin{bmatrix} T^{-1} & 0 \\ -D^{-1}CT^{-1} & D^{-1} \end{bmatrix} \cdot \begin{bmatrix} I & -BD^{-1} \\ 0 & I \end{bmatrix} = \begin{bmatrix} T^{-1} & -T^{-1}BD^{-1} \\ -D^{-1}CT^{-1} & D^{-1}CT^{-1}BD^{-1} + D^{-1} \end{bmatrix}$$
$$= \begin{bmatrix} A^{-1} + A^{-1}B\left(D - CA^{-1}B\right)^{-1}CA^{-1} & -A^{-1}B\left(D - CA^{-1}B\right)^{-1} \\ -\left(D - CA^{-1}B\right)^{-1}CA^{-1} & \left(D - CA^{-1}B\right)^{-1} \end{bmatrix} \tag{A.8}$$

Comparing a (1,1) block matrix in M^{-1} matrix, the Sherman-Morrison-Woodbury-Schur formula follows.

$$\left(A - BD^{-1}C\right)^{-1} = A^{-1} + A^{-1}B\left(D - CA^{-1}B\right)^{-1}CA^{-1} \tag{A.9}$$

Deriving the Kalman gain matrix in Section 3.7.2, one sets some variables as follows.

$$A \equiv \Sigma_0^{-1} \ , \ B \equiv -A_1^T \ , \ C \equiv A_1 \ , \ D \equiv \Sigma_{l,1}$$
$$\therefore \left(A_1^T \Sigma_{l,1}^{-1} A_1 + \Sigma_0^{-1}\right)^{-1} = \left\{ \Sigma_0 \ - \Sigma_0 \ A_1^T \left(A_1 \Sigma_0 \ A_1^T + \Sigma_{l,1} \ \right)^{-1} A_1 \Sigma_0 \ \right\} \tag{A.10}$$

REFERENCES

Brown, R.G., Hwang, P.Y.C., (1997): *Introduction to Random Signals and Applied Kalman Fitering*, John Wiley&Son.

Coco, R., (1991): GPS-satellite of Opportunity for Ionospheric Monitoring. *GPS World*, Vol. 2, No.9, pp. 47-50.

Gibson, R., (1983): A Derivation of Relativistic Effects in Satellite Tracking. *Technical report*, TR 83-55, Naval Surface Weapons Center, Dahlgren, Virginia.

Goad, C.C., Goodman, L., (1974): A Modified Hopfield Tropospheric Refraction Correction Model. Presented at the Fall Meeting of the American Geophysical Union, San Francisco, December, 1974.

Goad, C.C., Yang, M., (1995): A New Approach to Precision Airborn GPS Positioning for Photogrammetry. *Photogrammetric Engineering and Remote Sensing*, Vol. 63, No. 9, pp. 1067-1077.

Graviss, L.P., (1992): GPS development program status. In: Proceedings of ION GPS-92, Fifth International Technical Meeting of the Satellite Division of the Institute of Navigation, Albuquerque, New Mexico, September 16-18, 3-16.

Han, S., Rizos, C., (1996): Improving the Computational Efficiency of the Ambiguity Function Algorithm, *Journal of Geodesy*, Vol. 70, pp. 330-341.

Heroux, P., Kouba, J., (1995): GPS Precise Point Positioning with a Difference, Presented at Geomatics '95, Ottawa, Ontario, Canada, June 13-15.

Hofmann-Wellenhof, B., Lichtenegger, H., Collins, J., (1997): *GPS Theory and Practice*, Springer, New York.

IGS 900-second orbit and clock (1999): ftp://cddisa.gsfc.nasa.gov/pub/gps/products.

Janes, H.W., Langley, R.B., Newby, S.P., (1989): A Comparison of Several Models for the Prediction of Tropospheric Propagation Delay, In: Proceedings of the Fifth International Geodetic Symposium on Satellite Positioning, Las Cruces, New Mexico, March 13-17, Vol. 2: 777-788.

Jefferson, D.C., Heflin, M.B., Watkins, M.M., Webb, F.H., Zumberge, J.F., Bar-Server, Y.E., (1996): Jet Propulsion Laboratory IGS Analysis Center Report, 1996, in International GPS Service for Geodynamics 1996 Annual Report, J.F. Zumberge, D.E. Fulton, and R.E. Neilan, eds., JPL Publication 97-20, Pasadena, CA, 1997.

Jorgesen, P.S., (1984): Navstar / Global Positioning System 18-satellite Conatellations, Global Positioning System. Special Issue of Navigation, Vol. II.

JPL 30-second orbit and clock (1999): ftp://sideshow.jpl.nasa.gov/pub/jpligsac/hirate.

Kleusberg, A., Teunissen, P.J.G., (1996): *GPS for Geodesy*, Springer-Verlag, Berlin.

Koch, K.R., (1997): *Parameter Estimation and Hypothesis in Linear Models*, Springer, Berlin.

Lachapelle, G., Cannon, M.E., Qiu, W., Varner, C., (1996): Precise Aircraft Single-point Positioning Using GPS Post-mission Orbits and Satellite Clock Corrections. *Journal of Geodesy*, Vol. 70, pp. 562-571.

Leick, A., (1995): *GPS Satellite Surveying*, Wiley-Interscience.

Mader, G.L., (1990): Ambiguity Function Techniques for GPS Phase Initilization and Kinematic Solutions. In: Proceedings of the Second International Symposium on Precise Positioning with the Global Positioning System, Ottawa, Canada, September 3-7, pp. 1233-1247.

Mader, G.L., (1992): Rapid Static and Kinematic Global Positioning System Solutions Using the Ambiguity Function Technique, *Journal of Geophysical Research*, Vol. 97, pp. 3271-3283.

Martin, M.T.J., (1995): Estimation of Precise GPS Clock Bias Values, the ESOC IGS Analysis Centre.

Parkinson, B.W., Spilker, J.J., (1996): *Global Positioning System : Theory and Applications I*, Vol. 163, Progress in Astronautics and Aeronautics, AIAA.

Remondi, B.W., (1984): Using the Global Positioning System (GPS) Phase Observable for Relative Geodesy: Modeling, Processing, and the Results. University of Texas at Austin, Center for Space Research.

Remondi, B.W., (1985): Global Positioning System Carrier Phase: Description and Use. NOAA Technical Memorandum NOS NGS-42.

Remondi, B.W., (1989): Extending the National Geodetic Survey Standard GPS Orbit Formats. National Information Center, Rockville, Maryland, *NOAA Technical Report* NOS 133, NGS 46.

Remondi, B.W., (1990a): Pseudo-kinematic GPS Results Using the Ambiguity Function Method. National Information Center, Rockville, Maryland, NOAA Technical Memorandum NOS NGS-52.

Remondi, B.W., (1991): NGS Second Generation ASCII and Orbit Formats and Associated Interpolation Studies. Paper Presented at the XX General Assembly of the IUGG at Vienna, Austria, August 11-24.

Seeber, G., (1993): *Satellite Geodesy*, Walter de Gruyter, Berlin New York.

Shum, C.K., Yi, Y., Zhao, C., Parke, M., Cheng, K., Lin, J., Snow, K., Tseng, H., Martin, D., Mader, D., (1999): TOPEX SIDE B Altimeter Calibration/validation, First Calibration / Validation Workshop on TOPEX Side B Altimeter, Room A128, Building 33 Division 970 Conference room NASA/GSFC Greenbelt, Maryland, April 22-23, 1999.

Spilker, J.J., (1978): GPS Signal Structure and Performance Characteristics, *Navigation*, Vol. 25, p. 121-146.

Wooden, W.H., (1985): Navstar Global Positioning System: 1985. In: Proceedings of the First International Symposium on Precise Positioning with the Global Positioning System, Rockville, Maryland, April 15-19, Vol. 1, pp. 23-32.

Young, L.E., Neilan, R.E., Bletzacker, F.R., (1985): GPS Satellite Multipath: an Experimental Investigation. In: Proceeding of the First International Symposium on Precise Positioning with the Global Positioning System, Rockville, Maryland, April 15-19, Vol. 1, pp. 423-432.

Zumberge, J.F., Watkins, M.M., Webb, F.H., (1998): Characteristics and Applications of Precise GPS Clock Solutions Every 30 Seconds. *Journal of The Institute of Navigation*, Vol. 44, No. 4.